HHS Public Access

Author manuscript

Nature. Author manuscript; available in PMC 2021 December 01.

Published in final edited form as:

Nature. 2021 June ; 594(7863): 403–407. doi:10.1038/s41586-021-03593-1.

Intercalated amygdala clusters orchestrate a switch in fear state

Kenta M. Hagihara[#1,2], **Olena Bukalo**[#3], **Martin Zeller**[4], **Ayla Aksoy-Aksel**[4,5], **Nikolaos Karalis**[1], **Aaron Limoges**[3], **Tanner Rigg**[3], **Tiffany Campbell**[3], **Adriana Mendez**[3], **Chase Weinholtz**[3], **Mathias Mahn**[1], **Larry S. Zweifel**[6,7], **Richard D. Palmiter**[8,9], **Ingrid Ehrlich**[4,5], **Andreas Lüthi**[#1,2], **Andrew Holmes**[#3]

[1] Friedrich Miescher Institute for Biomedical Research, Maulbeerstrasse 66, 4058 Basel, Switzerland

[2] University of Basel, 4000 Basel, Switzerland

[3] Laboratory of Behavioral and Genomic Neuroscience, National Institute on Alcohol Abuse and Alcoholism, NIH, Bethesda, MD, USA

[4] Hertie Institute for Clinical Brain Research and Center for Integrative Neuroscience, 72076 Tübingen, Germany

[5] Department of Neurobiology, Institute for Biomaterials and Biomolecular Systems, University of Stuttgart, 70569 Stuttgart, Germany

[6] Department of Psychiatry and Behavioral Sciences, University of Washington, Seattle, WA, USA

[7] Department of Pharmacology, University of Washington, Seattle, WA, USA

[8] Howard Hughes Medical Institute, University of Washington, Seattle, WA USA

[9] Departments of Biochemistry and Genome Sciences, University of Washington, Seattle, WA, USA

[#] These authors contributed equally to this work.

Summary

Adaptive behaviour necessitates that memories are formed for fearful events, but also that these memories can be extinguished. Effective extinction prevents excessive and persistent reactions to perceived threat, as can occur in anxiety and ‘trauma- and stressor-related’ disorders[1]. However, while there is evidence that fear learning and extinction are mediated by distinct neural circuits, the nature of the interaction between these circuits remains poorly understood[2–6]. Here, through

correspondence should be addressed to A. Lüthi. and A. Holmes.

Author contributions

K.M.H., O.B., A.Lüthi., and A.H. conceived the project. K.M.H performed all the calcium imaging experiments, virus-based circuit mapping, and the slice experiments in Fig. 4e–j, Extended Data Fig. 11, 12 and analysed the data. O.B. performed chemogenetic manipulation experiments and analysed the data with A.Limoges, T.R., T.C., A.M., and C.W.. M.Z. and A.A.A performed the slice experiments in Fig. 4a–d, Extended Data Fig.7, 10 and analysed the data. I.E. conceived slice experiments and supervised M.Z. and A.A.A.. N.K. performed fibre photometry with K.M.H.. M.M. helped establishing the slice physiology setup and provided K.M.H. with technical training and advice on opsin selection. L.S.Z. and R.D.P. provided the FoxP2-Cre mouse line. K.M.H. prepared figures and drafted the manuscript. K.M.H., A.Lüthi., and A.H. wrote the manuscript. All the authors commented on and finalized the manuscript and figures. A.Lüthi. and A.H. supervised the entire project.

Competing interests

The authors declare no competing interests.

a combination of *in vivo* calcium imaging, functional manipulations, and slice physiology, we demonstrate that distinct inhibitory clusters of intercalated neurons (ITCs) located in the amygdala exert diametrically opposite roles during the acquisition and retrieval of fear extinction memory. Furthermore, we find that the ITC clusters antagonize one another via mutual synaptic inhibition and differentially access functionally distinct cortical- and midbrain-projecting amygdala output pathways. Our findings show that the balance of activity between ITC clusters represents a unique regulatory motif orchestrating a distributed neural circuitry regulating the switch between high and low fear states. This suggests a broader role for the ITCs in a range of amygdala functions and associated brain states underpinning the capacity to adapt to salient environmental demands.

Animals are equipped with biological systems to detect and defend against environmental threats. Through associative learning, stimuli predicting threat mobilize defensive responses to mitigate harm[7]. When threat-associated stimuli become innocuous, responses adapt through the process of extinction, whereby a new memory is formed that coexists in opposition to the original fear memory[4,8,9]. Specialized neural systems have evolved to subserve fear and extinction which, when imbalanced, cause persistent reactions to threat.

ITC clusters are densely packed GABAergic neurons surrounding the basolateral amygdala (BLA), distinguished from neighbouring neurons by their electrophysiological and molecular properties[10–13]. The medial ITC clusters, located in the intermediate capsule at the BLA-central amygdala (CeA) junction, receive BLA input and modulate CeA activity through feed-forward inhibition[2,14] in a manner potentiated by extinction[15]. Though medial ITC ablation impairs extinction[16], recent studies suggest functional[10] and anatomical[17,18] heterogeneity between medial ITC clusters. However, given their small size and location deep in the brain, elucidating ITC cluster functions has proven challenging.

ITC clusters signal an aversive stimulus

We employed *in vivo* deep-brain imaging to monitor Ca^{2+} activity in individual ITC neurons in freely-moving mice, via a miniaturized microscope[19]. We separately targeted neurons in the dorsal cluster ITC_{dm} and ventral cluster ITC_{vm} (corresponding to previously defined Imp and IN[10], respectively; for detailed anatomical demarcation of the clusters, see Extended Data Fig. 1, Supplementary Movie 1, and Supplementary Table 1). To target ITC_{dm}, BLA, and CeA, an adeno-associated virus (AAV) encoding a Ca^{2+} indicator, GCaMP6f, was injected into amygdala (Extended Data Fig. 2a–c), and a graded refractive index (GRIN) lens implanted (Fig. 1a,b). To isolate ITC_{dm} Ca^{2+} responses, we selected IHC-labelled FoxP2+ neurons from GRIN lens images for analysis by registering maximum intensity projection Ca^{2+} images to 3D confocal images of cleared tissue (Fig. 1c–e, Supplementary Movie 2, see Methods).

Implanted mice were tested in a 5-day fear conditioning/extinction paradigm (see Methods and Fig. 2a). We first limited analysis to shock-evoked Ca^{2+} responses during fear conditioning (Day2) – comprising 5 pairings of an auditory conditioned stimulus (CS) with a footshock unconditioned stimulus (US). Footshocks reliably elicited strong responses in ITC_{dm} neurons (Fig. 1f,g,j, Extended Data Fig. 2d, Supplementary Movie 3) whereas simultaneously recorded neurons in CeA and BLA exhibited sparse and

heterogeneous responses (Fig. 1f,g, Extended Data Fig. 2d). *In vivo* 2-photon Ca^{2+} imaging performed in head-fixed mice, providing higher spatial resolution and simultaneous cell-type identification, confirmed most ITC_{dm} neurons responded to shock (84.5%, 93/110 neurons, N=5 mice, Extended Data Fig. 3a–e). By contrast, ITC_{vm} neurons did not show footshock responses (Fig. 1h–j, Extended Data Fig. 2e–h). The fraction of shock-responsive ITC_{vm} neurons was smaller than for ITC_{dm} ($P = 1.6 \times 10^{-48}$, Chi-squared test). ITC_{dm}, not ITC_{vm}, activity was also highly correlated during conditioning and a home-cage session (Extended Data Fig. 2i–n). Furthermore, dual-colour *in vivo* fibre photometry simultaneously measuring activity of ITC_{dm} and ITC_{vm} projections in BLA found their activity was largely anti-correlated (Extended Data Fig. 3f–j).

As extinction is based on the absence of an expected aversive stimulus[20,21], and ITCs are ascribed a role in extinction[2,16], we asked whether the clusters differentially respond to shock omission. We examined extinction training (Day3, see Methods and Fig. 2a), where the CS was presented without the US (25x), and aligned Ca^{2+} traces to CS-offset (when footshocks were delivered during conditioning). During the first 5 CS/no-US trials, the fraction of neurons responding to US-omission was greater in ITC_{vm} (28%) than ITC_{dm} (4%; $P=5.8 \times 10^{-15}$, Chi-squared test), as was the average size of the response (Fig. 1k,l, Extended Data Fig. 3k,l). On late extinction training (trials 21–25), shock-omission responses in ITC_{vm} were markedly reduced, consistent with representing deviations from expectation.

These data demonstrate ITC_{dm} and ITC_{vm} neurons oppositely represent the presence and absence of an aversive stimulus. Opposing functional profiles likely reflect differential connectivity with upstream brain regions; e.g., ITC_{dm} shock responses could be driven by multisensory and pain processing areas, including the medial geniculate nucleus/posterior intralaminar nucleus thalamic complex[17,22].

ITC clusters track fear state switches

Do ITC clusters exhibit differential fear state-dependent responses to conditioned CSs? We measured Ca^{2+} activity in ITC_{dm} and ITC_{vm} neurons during CS/context habituation (Day1), CS-US conditioning (FC, Day2), CS-only extinction training (Ext1, Day3, Ext2, Day4) and extinction retrieval (Retrieval, Day5) (Fig. 2a, see Methods). CS-elicited freezing, a readout of fear state, increased over conditioning and was maintained at fear retrieval (early extinction Day3 trials) before decreasing with extinction training, and remaining low on extinction retrieval (Fig. 2b).

We functionally classified ITC neurons into three mutually exclusive categories (as for BLA neurons[23]). Fear neurons were selectively active during fear retrieval/early extinction, Extinction neurons developed responses by late extinction, and Extinction-resistant neurons showed sustained activity across extinction training (Fig. 2c, Extended Data Fig. 4a–c, see Methods). ITC_{dm} contained a large fraction of Fear neurons (75% CS-responsive/32% recorded), but a small fraction of Extinction neurons (15% CS-responsive/6% recorded, $P<0.01$) (Fig. 2d, Extended Data Fig. 4d). Conversely, Extinction neurons were overrepresented in ITC_{vm} (74% CS-responsive/18% recorded), with a much

smaller fraction of Fear neurons (18% of CS-responsive/5% of recorded). There was only a small fraction (<5%) of Extinction-resistant neurons in each cluster.

Examining response dynamics revealed most ITC_{dm}-Fear neurons showed an onset-locked CS response during early extinction, suggesting rapid detection of the CS's aversive properties. CS responses were much reduced at extinction retrieval (Fig. 2e). Conversely, CS-responses in ITC_{vm}-Extinction neurons emerged by the second extinction training session (Day4) and were maintained on extinction retrieval (Day5) (Fig. 2e). This delayed increases suggests prolonged extinction training and/or overnight extinction consolidation is required to recruit ITC_{vm}-Extinction neurons (as in BLA[23]).

Further indicating divergent activity in the clusters, the overall amplitude of CS-responses positively correlated with freezing in ITC_{dm}-Fear neurons, but anti-correlated with freezing in ITC_{vm}-Extinction neurons (Fig. 2f,g). These correlations were not evident at freezing onset and offset specifically (Extended Data Fig. 5a). Importantly, these relationships held when considering all recorded (not only classified) neurons (Extended Data Fig. 5b,c). ITC_{vm} neurons did not show tone responses on habituation (Day1), indicating ITC_{vm} activity does not simply reflect a low fear state, but represents a diminished fear state produced by extinction (Extended Data Fig. 5d). In contrast, ITC_{dm} neurons showed tone responses on habituation (Day1), which rapidly reduced across 5 trials, suggesting a habituation-like response to novelty (Extended Data Fig. 5e).

When aligning responses to US-omission, ITC_{vm}-Extinction, but not ITC_{dm}-Fear neurons showed strong responses (Extended Data Fig. 5f). This is consistent with the shock-omission responses observed for the entire recorded ITC_{vm} population on test Day3 (Fig. 1k,l), which had decreased by Day5 (Extended Data Fig. 5g). Indeed, US-omission responses were weakly positively correlated with extinguished (Day4) CS-responses (R = 0.36), suggesting functional overlap between ITC_{vm} neurons signalling US-omission and extinction (Extended Data Fig. 5h). Hence, a prevailing fear state is represented by the relative balance of ITC_{dm} and ITC_{vm} neuron activity.

To assess whether interplay between ITC clusters is evident in other situations characterized by a shift in behavioural state, we used dual-cluster *in vivo* fibre photometry to simultaneously record ITC_{dm} and ITC_{vm} Ca^{2+} activity in an elevated zero-maze (Extended Data Fig. 6a). Transitions between quadrants corresponded to a marked shift in the balance of activity in the two clusters; ITC_{vm} activity increased during transitions from the protected, closed, to the unprotected, open, quadrants (Extended Data Fig. 6b–e). This increase might serve to inhibit defensive behaviour and enable open quadrant exploration, analogous to the inhibition of freezing following extinction. Hence, these data suggest shifts in ITC cluster activity correspond to transitions between defensive and explorative behavioural states across paradigms.

ITC clusters regulate fear extinction

We next assessed the causal effects of manipulating the balance of ITC cluster activity, using *in vivo* chemogenetics. A Cre-dependent form of the Gi-coupled kappa-opioid

receptor DREADD (KORD) was expressed in ITC_{dm} or ITC_{vm} of FoxP2-Cre mice and Cre-negative controls (Fig. 3a–f). The pharmacologically inert ligand salvinorin B (SalB) was systemically injected to selectively inactivate either cluster (for functional verification via *ex vivo* neuronal recordings in acute brain slices and targeting success rates, and statistics, see Extended Data Fig. 7–9, Methods, and Supplementary Table 2).

ITC_{vm} inactivation during extinction training impaired extinction memory formation, as evidenced by higher CS-related freezing in Cre+ versus Cre− mice on (drug-free) extinction retrieval (Fig. 3b). In a separate experiment, ITC_{vm} inactivation during extinction retrieval, not acquisition, impaired retrieval (Fig. 3c). Thus, ITC_{vm} is necessary for extinction memory formation and retrieval. Next, we used the G_q-coupled DREADD, hM3Dq and systemic clozapine-n-oxide (CNO) injection to activate ITC_{vm} neurons during extinction retrieval (Fig. 3d). Using a partial extinction training protocol (avoiding freezing floor effects, see Methods), we found activating ITC_{vm} decreased CS-related freezing, relative to Cre− controls, indicating facilitated extinction retrieval. Importantly, selectively expressing hM3Dq or KORD in ITC_{dm} and administering CNO or SalB to respectively activate or inactivate ITC_{dm} during extinction retrieval produced effects opposite to these same manipulations in ITC_{vm}. Specifically, relative to Cre− controls, ITC_{dm} activation increased (Extended Data Fig. 9a,b), whereas ITC_{dm} inactivation decreased, CS-related freezing in Cre+ mice on retrieval (Fig. 3e,f). Finally, when we expressed KORD in ITC_{dm} as well as ITC_{vm} and injected SalB prior to extinction retrieval, retrieval was impaired (Extended Data Fig. 9c–f), consistent with prior evidence that medial cluster-wide pre-retrieval toxin-lesioning impairs extinction retrieval in rats[16].

Collectively, these data strongly align with our imaging results showing Fear and Extinction neurons were overrepresented (albeit not exclusively) in ITC_{dm} and ITC_{vm}, respectively.

ITC clusters are mutually inhibitory

We next tested whether the balance of activity between ITC_{dm} and ITC_{vm} was determined by mutual inhibitory interactions. Injecting an AAV expressing Cre-dependent synaptophysin-GFP to target ITC_{dm} or ITC_{vm} in FoxP2-Cre mice (Extended Data Fig. 10a) revealed strong axonal projections and putative synaptic connections in both directions. We saw no somatic expression in projection-target areas, excluding injection leakage and transsynaptic infection (Extended Data Fig. 10b,c). To test for functional GABAergic mono-synaptic connections, we infected ITC_{dm} or ITC_{vm} with an AAV encoding Cre-dependent channelrhodopsin-2 (ChR2) (Extended Data Fig. 10d,e) and photostimulated ChR2-expressing axons in acute brain slices while performing whole-cell patch-clamp recordings of neurons located in the non-injected cluster (Fig. 4a).

There were synaptic connections in all recorded ITC neurons (ITC_{vm}→ITC_{dm}: n=15/15; ITC_{dm}→ITC_{vm}: n=14/14), demonstrating dense inter-cluster reciprocal connectivity. Optically-evoked synaptic responses were blocked by the $GABA_A$-receptor blocker picrotoxin, and exhibited reversal potentials close to the equilibrium potential for chloride, confirming they were GABAergic IPSCs (Fig. 4b,c, Extended Data Fig. 10f). Synaptic responses persisted on application of the sodium channel blocker tetrodotoxin and potassium

channel antagonist 4-AP, demonstrating monosynaptic connectivity (Fig. 4b,d). Using spatially-focused light to directly stimulate individual clusters confirmed these results (Extended Data Fig. 10g–l). Thus, ITC_{dm} and ITC_{vm} are reciprocally and monosynaptically connected by functional inhibitory synapses.

ITC clusters control amygdala outputs

Interconnectivity between ITC_{dm} and ITC_{vm} could provide a mechanism regulating shifts in cluster activity to orchestrate extinction via effects on downstream pathways. To explore this idea, we expressed a Cre-dependent, GFP-fused and soma-targeted opsin, soCoChR-EGFP, in ITC_{dm} and ITC_{vm} of FoxP2-Cre mice (Extended Data Fig. 11a), and selectively photostimulated each cluster in acute brain slices via two thin-fibre-coupled LEDs (Fig. 4e, Extended Data Fig. 11b–k). Stimulation of ITC_{vm} (73% of recorded) but much less so ITC_{dm} (9% of recorded) neurons evoked a postsynaptic response in medial CeA (CeM), a known ITC target[24] (Extended Data Fig. 12a–e). Within CeM, ventrolateral periaqueductal gray (vlPAG)-projecting neurons, a fear-promoting pathway[25], preferentially received inhibitory input from ITC_{vm} (Extended Data Fig. 12f–i).

Next, we examined ITC outputs to BLA[10,17,18], focusing on IL- and PL-projecting neurons given prior evidence that these populations represent extinction-promoting and extinction-opposing BLA output pathways, respectively[26]. After selectively labelling each population with the retrograde tracer cholera toxin B (CTB) (Extended Data Fig. 12j–m, see Methods), we recorded CTB+ (and neighbouring CTB−) BLA neurons while optically stimulating ITC_{vm} or ITC_{dm}. This revealed GABAergic (picrotoxin-sensitive) connections from ITC_{vm} to PL-projecting BLA neurons and from ITC_{dm} to IL-projectors, but not *vice versa* (Fig. 4f–h). Connections from ITC_{dm} to IL-projecting BLA neurons were also stronger than those from ITC_{vm} to BLA PL-projectors (Fig. 4i,j).

These data demonstrate a double dissociation in connectivity from specific ITC clusters to distinct amygdala output pathways. Fear-promoting BLA→PL and CeM→vlPAG pathways are more strongly inhibited by ITC_{vm} than ITC_{dm}, whereas ITC_{dm} makes inhibitory inputs onto the extinction-promoting BLA→IL pathway (Extended Data Fig. 12n). mPFC-projecting BLA neurons preferentially contact IL and PL neurons that project back to BLA[27], and these mPFC→BLA projections are differentially involved in fear extinction[28]. Thus, ITC_{dm} and ITC_{vm} clusters have specific and direct access to major cortico-amygdala loops regulating fear extinction.

Discussion

Brain mechanisms enabling an appropriate balance between avoiding threat-predicting stimuli and suppressing excessive defensive behaviour after uneventful encounters are critical to survival. Here, we show the ITC clusters located in the intermediate capsule boundary between BLA and CeA provide a substrate for achieving this balance during fear extinction. The relative weighting of ITC cluster activity also reflected exploration of protected and unprotected areas in the elevated zero-maze. Hence, dynamic changes in the

balance of ITC activity may be a general feature of behavioural state shifts occurring during significant changes in the environment.

The ITC_{dm} and ITC_{vm} clusters form a mutually inhibitory network precisely accessing functionally distinct amygdala output pathways to orchestrate a broader circuitry underlying a switch in defensive states. Direct mutual inhibitory connections between ITC clusters offer an efficient mechanism subserving shifts in relative activity in response to experience with the CS, such that a weighting favouring $ITC_{dm} \rightarrow ITC_{vm}$ interactions during fear retrieval is dynamically transformed to $ITC_{vm} \rightarrow ITC_{dm}$ inhibition with extinction. This dynamic process may be modulated by, as yet unidentified, upstream regions conveying information to the ITCs about the sensory and valence properties of the CS and US. Though dissociable neuronal populations and subregions in other brain regions are known to exert opposite effects on extinction[3–5], the ITCs appear unique in accommodating mutual inhibition as spatially separated inter-cluster connectivity.

A mutually inhibitory motif could amplify small differences in input to an all-or-none output pattern, providing a ‘winner-take-all’ mechanism enhancing signal-to-noise to generate robust ITC circuit-output and associated behavioural states[29,30]. Accordingly, ITCs could serve as a low-dimensional interpreter of sensory, cognitive and emotional information to orchestrate amygdala functions and associated brain states underpinning adaptation to salient environmental demands. ITC neurons could thereby influence a wide-range of amygdala-mediated behaviours, including states associated with positive valence, which have overlapping neural representations with fear extinction[31–33]. Finally, given ITCs are present in human brain[34] aberrant ITC function could contribute to susceptibility to various psychiatric conditions.

Methods

Mice

All animal procedures were performed in accordance with institutional guidelines and with current European Union guidelines, and were approved by the Veterinary Department of the Canton of Basel-Stadt, Switzerland, by the local government authorities for Animal Care and Use (Regierungspräsidium Tübingen, State of Baden-Württemberg, Germany), and by the NIAAA Animal Care and Use Committee. FoxP2-IRES-Cre mice (JAX#030541)[35] were used for Cre-dependent expression of viral vectors. For some experiments where a Cre-dependent expression system was not required, Arc-CreER mice[36] crossed with a tdTomato reporter line (Ai14) were used in addition to wild-type C57BL/6J mice. For 3D reconstruction, FoxP2-IRES-Cre mice crossed with Ai14 and D1R-Cre (JAX#37156) mice crossed with Ai14 were used. All lines were backcrossed to C57BL/6J. For behavioural experiments, only male mice (aged 1.5–3 months old at the time of virus injection) were used. Both male and female mice (2–5 months old at the time of injection, unless otherwise noted) were used for virus-based circuit tracings, *ex vivo* electrophysiology and immunohistochemistry. These analyses indicated no discernible differences between males and females; however, more detailed studies will be needed to examine potential sex differences in ITC circuit anatomy and function. Mice were individually housed for at least two weeks before starting behavioural paradigms. Animals were kept in a 12-h light/dark

cycle with access to food and water *ad libitum*. All behavioural experiments were conducted during the light cycle.

Surgical procedures and viral vector injections

Buprenorphine (Temgesic, Indivior UK Limited; 0.1 mg/kg BW) was injected subcutaneously 30 min prior to the surgery. Mice were anesthetized using isoflurane (5% for induction, 1–2% for maintenance; Attane, Provet) in oxygen-enriched air (Oxymat 3, Weinmann) and then head-fixed on a stereotactic frame (Model 1900, Kopf Instruments). Lidocaine + Ropivacain (Lidocain HCl, Bichsel, 10mg/kg BW; Naropin, AstraZeneca, 3mg/kg BW) were injected subcutaneously as local anesthesia prior to incision to the skin. Postoperative pain medication included buprenorphine (0.01 mg/ml in the drinking water; overnight) and injections of meloxicam (Metacam, Boehringer Ingelheim; 5 mg/kg subcutaneously) for up to three days if necessary. Eyes were protected with ophthalmic ointment (Viscotears, Alcon). Rectal body temperature of the animal was maintained at 35–37°C using a feedback-controlled heating pad (FHC) while fixed on the stereotactic frame.

Deep brain imaging: AAV2/5.CaMK2.GCaMP6f[37] (600 nl, University of Pennsylvania Vector Core, UPenn, for simultaneous imaging of CeA, ITC_{dm}, and BLA) or AAV2/9.CAG.flex.GCaMP6f (200 nl, University of Pennsylvania Vector Core, UPenn, for ITC_{vm}) was unilaterally injected into the amygdala using a precision micropositioner (Model 2650, Kopf Instruments) and pulled volume-calibrated glass capillaries (Drummond Scientific, Cat.-No. 2–000-001, tip diameter about 15 μm) connected to a Picospritzer III microinjection system (Parker Hannifin Corporation) at the following coordinates; For ITC_{dm}: AP −1.4 mm (from bregma), ML −3.3 mm (from bregma), DV 4.4 mm (from pia); For ITC_{vm}: AP −1.6 mm (from bregma), ML −3.1 mm (from bregma), DV 5.0 mm (from pia); After waiting at least 10 min for diffusion of the virus, a gradient-index microendoscope (ITC_{dm}: φ1.0 × 9.0 mm, 1050–002179, Inscopix GRIN lens; ITC_{vm}: φ0.6 × 7.3 mm, 1050–002177, Inscopix GRIN lens) was implanted. The larger diameter lens was used to record from ITC_{dm} 1) to increase the probability of capturing this relatively small cluster in the field of view and 2) to provide simultaneous recordings from BLA and/or CeA neurons from the same lens. The smaller diameter lens was used to record from ITC_{vm} to reduce damage to the overlying CeA. For dual-colour 2-photon imaging, a cocktail of AAV2/5.CaMK2.GCaMP6f and AAV2/1.CAG.FLEX.tdTomato (University of Pennsylvania Vector Core, UPenn) (600nl, 10–20:1 mixture ratio) was unilaterally injected targeting ITC_{dm}. A sterile 21-gauge needle was used to make an incision above the imaging site to avoid excessive brain pressure. The GRIN lens was subsequently lowered into the brain with a micropositioner (coordinates; For ITC_{dm}: AP −1.4 mm, ML 3.25 mm, DV 4.35 mm (from pia); For ITC_{vm}: AP −1.6 mm, ML 3.0 mm, DV 4.8 mm (from pia)) using a custom-built lens holder and fixed to the skull using UV light-curable glue (Henkel, Loctite 4305). Surface of the skull was sealed with Vetbond (3M). Dental acrylic (Paladur, Heraeus) was used to further seal the skull and attach a custom-made titanium head bar for fixation during the miniature microscope mounting procedure. The implanted GRIN lens was protected by rapid-curing silicone elastomers.

Chemogenetic manipulation: AAV2/8(the genome of serotype 2 packaged in the capsid from serotype 8).hSyn.KORD.IRES.mCitrine[38] (Addgene plasmid # 65417, packaged by Virovek (Hayward, CA, USA)) or AAV2/8.hSyn.DIO.hM3D(Gq)-mCherry[39] (Addgene viral prep # 44361-AAV8) was bilaterally injected to FoxP2-Cre experimental animals (Cre+) and Cre− control animals in a volume of 0.15 μL per hemisphere for individual clusters or 0.25 μL per hemisphere for both medial clusters with a 0.5 μL syringe (Neuros model 7001 KH, Hamilton Robotics, Reno, NV, USA) connected to a UMP3 UltraMicroPump and SYS-Micro4 Controller or Nanoliter NL2010MC4 injector (World Precision Instruments, LLC, Sarasota, FL, USA) at the following coordinates; for ITC_{dm} targeting: AP −1.4 mm, ML ±2.95 mm, DV −4.55 mm (from bregma); for ITC_{vm} targeting: AP −1.55 mm, ML ±2.75 mm, DV −5.15 mm; for dual ITC_{dm} and ITC_{vm} targeting: AP −1.43 mm, ML ±2.75 mm, DV −4.75 mm.

Virus-based circuit tracings: AAV2/1.hSyn.flex.synaptophysin-EGFP (packaged by VectorBiolabs, 10–25nl) was target-injected into either ITC_{dm} or ITC_{vm} (with the same coordinates as shown above) of FoxP2-IRES-Cre mice. Following viral injections, pipettes were left in place for 10 min and retracted slowly to better restrict virus infection. Three to five weeks after the injection, the animals were sacrificed for histological analysis.

Ex vivo electrophysiology: For KORD functionality assay (Extended Data Fig.7), AAV2/8.hSyn.KORD.IRES.mCitrine was injected targeting both medial ITC clusters in FoxP2-IRES-Cre mice as stated above. For inter-cluster connectivity assay (Fig. 4a–d, Extended Data Fig. 10), AAV2/1.EF1a.DIO.HChR2(H134R)-EYFP (U.Penn) was target-injected using a precision stereotactic frame (Model 1900, Kopf Instruments) into either ITC_{dm} or ITC_{vm} of FoxP2-IRES-Cre mice as noted above. For analysis of ITC-BLA connectivity (Fig. 4e–j), FoxP2-IRES-Cre mice were unilaterally injected into the amygdala with 500 nl of AAV2/9.hSyn.flex.soCoChR-EGFP[40] (Addgene # 107712-AAV9) (coordinates: AP −1.5 mm, ML ±3.15 mm, DV 4.2–5.0 mm (from pia)) so that both ITC_{dm} and ITC_{vm} would be infected. Mice were allowed to recover for 5–6.5 weeks for KORD functionality assay (Extended Data Fig.7), and for 2–4 weeks before *ex vivo* electrophysiology experiments (Fig. 4, and Extended Data Fig. 10). To retrogradely label PL- or IL-projecting BLA neurons, 50 nl of 0.5% cholera toxin B conjugated to either Alexa Fluor 555 or 647 (CTB555 or CTB647) was injected into the same hemisphere of the mPFC as the AAV injection at the following coordinates (for PL targeting: AP +1.55 mm, ML ±0.3 mm, DV 1.9 mm (from pia); for IL targeting: AP +1.75 mm, ML ±0.4 mm, DV 2.5 mm (from pia)). To label vlPAG-projecting CeM neurons, 100 nl of 0.2 % CTB555 in PBS were injected into the same side of the vlPAG as the AAV injection. To avoid the subcranial midline blood sinus while targeting the vlPAG, a hole with a diameter of 0.3 mm was drilled into the skull at ±1.7 mm from midline suture, and at the level of the lambda suture. The injection capillary was then slowly lowered at a zenith angle of 26° to the target depth of 3 mm below brain surface. CTB injections and AAV injections were performed in the same surgeries.

Fibre photometry recordings: ITC_{dm} and ITC_{vm} in the same hemisphere were targeted with 25 nl of AAV2/1.CAG.Flex.NES.jRGECO1a.WPRE[41]

(Addgene) and AAV2/1.CAG.Flex.jGCaMP7f.WPRE[42], respectively, or AAV2/1.CAG.Flex.jGCaMP7f.WPRE was injected to target left ITC_{dm} and right ITC_{vm}. Following virus injections, an optical cannula comprised of a bare optical fibre (φ 0.4) and a fibre ferrule (Doric Lenses) was implanted in the BLA (AP −1.4 mm, ML ±3.3 mm, DV 4.3 mm (from pia)) for unilateral recordings. For bilateral recordings, ITC_{dm} and ITC_{vm} clusters were directly targeted by two optical cannulas with the same coordinates as virus injections. The surface of the skull was sealed with Vetbond (3M). Dental acrylic (Paladur, Heraeus) was used to further seal the skull and attach a custom-made titanium head bar for fixation. The ferrules were protected by rapid-curing silicone elastomers.

Immunohistochemistry

Mice were deeply anaesthetized with urethane (2 g/kg; intraperitoneally) and transcardially perfused with PBS followed by 4% paraformaldehyde (PFA) in PBS. Brains were post-fixed over night at 4°C and subsequently stored in PBS at 4°C. Coronal slices (120 μm) containing the BLA were cut with a vibratome (VT1000S, Leica). Sections were washed in PBS for 10 min two times, permeabilized with permeabilization solution[43] (0.2% Triton X-100, 20% DMSO, and 23 g/L Glycine in PBS) for 30 min at 37°C, blocked in blocking solution (0.2% Triton X-100, 10% DMSO, and 6% normal donkey serum (NDS) in PBS) for 30 min at 37°C. Slices were subsequently incubated in primary antibody solution (1:2000 rabbit anti-FoxP2 (Abcam, ab16046), 5% DMSO, 3% NDS, 0.2% Triton X-100, 10 mg/L Heparin in PBS) for 24 h at 37°C. After washing for 10 min three times with 0.2% Triton X-100 in PBS, sections were incubated for 24 h at 37 °C with a secondary antibody solution (1:500 donkey anti-rabbit Alexa Fluor 647 (Thermo Fisher Scientific), 3% NDS, 0.2% Triton X-100, and 10 mg/L heparin in PBS. After washing at least 30 min three times in PBS, sections were mounted on gelatin-coated glass slides and covered with anti-fade mounting medium and coverslips. Sections were scanned using a laser scanning confocal microscope (LSM700, Carl Zeiss) equipped with a 5x air objective (Plan-Apochromat 5x/0.15NA), a 10x air objective (Plan-Apochromat 10x/0.45NA), 20x air objective (Plan-Apochromat 20x/0.8NA) or 63x oil objective (Plan-Apochromat 63x/1.4NA).

3D reconstruction

For 3D reconstruction, thick coronal sections (3–4 mm) containing all the ITC clusters were prepared with a vibratome (VT1000S, Leica). The sections were then cleared using the CUBIC protocol[44]. A subset of sections was also stained with the FoxP2 antibody. The cleared tissues were imaged with a confocal microscope (Zeiss, LSM700) equipped with a 10x air objective (Zeiss, C Epiplan-Apochromat 10x/0.40NA) or 20x air objective (Zeiss, LD Plan-NEOFLUAR, 20x/0.4NA), which have a relatively long working distance (> 5 mm). The voxel size was 1–3 um * 1–3 um * 10um (x*y*z) to achieve single-cell resolution. Acquired images were imported to Imaris software (Bitplane) and individual ITC clusters were manually reconstructed plane-by-plane with manual contour drawing function in ‘Measurement Pro’ package. Densely packed regions with marker positive neurons were regarded as clusters. Semi-transparent mouse brain scheme was created using Brainrender[45].

Deep brain calcium imaging

Miniature microscope imaging: Two to six weeks after GRIN lens implantation, mice were head-fixed to check for sufficient expression of GCaMP6 using a miniature microscope[46] (nVista HD, Inscopix). Mice were briefly anesthetized with isoflurane to fix the microscope baseplate (1050–002192, Inscopix) to the skull using blue light curable glue (Vertise Flow, Kerr). The microscope was removed and the baseplate was capped with a baseplate cover (1050–002193, Inscopix). Mice were habituated to the brief head-fixation on a running wheel for miniature microscope mounting for at least three days before the behavioural paradigm. Imaging data were acquired using nVista HD software (Inscopix) at a frame rate of 20 Hz with an LED power of 10–60% (0.9–1.7 mW at the objective, 475 nm), analogue gain of 1, and with 1080 × 1080 pixels. For individual mice, the same imaging parameters were kept across days. Timestamps of imaging frames and behavioural stimuli were collected for alignment using the Omniplex system (Plexon).

Fear conditioning and extinction paradigm: Two different contexts were used; Context A (extinction context) consisted of a clear cylindrical chamber (diameter: 23 cm) with a smooth floor, placed in a dark-walled sound attenuating chamber under dim light conditions. The chamber was scented and cleaned with 1% acetic acid. Context B (fear conditioning context) contained a clear square chamber (26.1 × 26.1 cm) with an electrical grid floor (Coulbourn Instruments) for footshock delivery, placed in a light-coloured sound attenuating chamber with bright light conditions, and was scented and cleaned with 70% ethanol. A stimulus isolator (ISO-Flex, A.M.P.I.) was used for the delivery of direct current (DC) shock. Both chambers contained overhead speakers for delivery of auditory stimuli, which were generated using a System 3 RP2.1 real time processor and SA1 stereo amplifier with RPvdsEx Software (all Tucker-Davis Technologies). Cameras (Stingray, Allied Vision) for tracking animal behaviour were also equipped in both chambers. Radiant Software (Plexon) was used to generate precise TTL pulses to control behavioural protocols and all the TTL signals including miniscope frame timings were recorded by Plex Control Software (Plexon) to synchronize behavioural protocols, behavioural tracking, and miniscope imaging.

On Day1 (Habituation), the mice were first imaged in their homecage for 10 min, and then placed in context A and exposed to 5 CSs (29 pips, 200 ms, 6-kHz pure tone, repeated at 1 Hz) following a 4-min baseline period. The ITI (inter tone interval) was 30 s. On Day2 (fear conditioning), mice were first imaged in their homecage for 10 min, and then fear conditioned in context B by pairing 5 CSs with an unconditioned stimulus (US; 1-s footshock, 0.65 mA DC; applied 800 ms after termination of the last (29th) pip) with a variable ITI of 60–90 s (after a 2-min baseline period). Animals remained in context B for 1 min after the last CS-US pairing. On Day3 and Day4 (extinction 1 and 2), fear memory was extinguished in context A. After a 4-min baseline period, animals were exposed to 25 CSs (ITI: 30 s). On Day5, extinction memory was assessed with 5 CS presentations (ITI: 30 s) following a 4-min baseline period.

Verification of implant sites (clearing-based, for ITC_{dm}): Upon completion of the behavioural paradigm, mice were lightly anesthetized with isoflurane, head-fixed and 3D-

scanned with a 2-photon microscope (Ultima, Bruker) equipped with a Ti:Sapphire laser (Insight X3, Spectra Physics) and a 16x water objective lens (0.8NA, Nikon) or 25x water objective lens (1.05NA, Olympus), through the GRIN lens. After 2-photon microscopy, mice were transcardially perfused (as above). GRIN lenses and head bars were removed and brains were post-fixed in 4% paraformaldehyde overnight at 4°C. Horizontal thick sections (1.5–2.0 mm) containing the imaging site were cut with a vibratome (VT1000S). Sections were cleared and stained against FoxP2 using the CUBIC protocol[44] and the same combination of antibodies as above, and then imaged with a confocal microscope (Zeiss, LSM700) equipped with a 5x air objective (Zeiss, Plan-Apochromat 5x/0.15NA) or 20x air objective (Zeiss, LD Plan-NEOFLUAR, 20x/0.4NA), which have a relatively long working distance. Using blood vessels and fibres as landmarks, a maximum intensity projection of the movie acquired with a miniature microscope, a 3D stack acquired with the 2-photon microscope, and a 3D stack acquired with confocal microscopy were manually matched, and then, the area of the miniature microscope movie corresponding to FoxP2-positive area between BLA and CeA in the confocal image were assigned as ITC_{dm}. Mice with obvious misplacement of the GRIN lens and with no FoxP2 signal were excluded from the analysis. For cases in which CeA was imaged in the periphery of the FOV, only data from ITC_{dm} and BLA were analysed.

Verification of implant sites (slice-based, for ITC_{vm}): Upon completion of the behavioural paradigm, mice were transcardially perfused (as above). GRIN lenses and head bars were removed, and brains were post-fixed in 4% paraformaldehyde overnight at 4°C. Coronal sections (120 μm) containing the imaging site were cut with a vibratome (VT1000S), immediately mounted on glass slides and coverslipped. To verify the GRIN lens position, sections were imaged with a confocal microscope as described above. Images were matched against a mouse brain atlas[47]. Mice with misplacement of the GRIN lens were excluded from the analysis.

2-photon calcium imaging: In a subset of mice used for miniature microscope experiments, awake head-fixed 2-photon imaging sessions were performed through the same implanted GRIN lenses using a 2-photon microscope (Ultima Investigator, Bruker) equipped with a Ti:Sapphire femtosecond laser (InSightX3, SpectraPhysics) and a 16x/0.8NA objective (N16XLWD-PF, Nikon). GCaMP6f and tdTomato were excited at 920 nm, and signals were filtered with a 517–567 nm band-pass filter and a 573–613 nm band-pass filter, respectively. Care was taken to shield the microscope objective and the photomultipliers from stray light. Images were obtained using Prairie View software (Bruker). Square regions (approximately 800 μm × 800 μm) were imaged at 512 × 512 pixels at 30 Hz with the resonant-galvo mode. Several planes were acquired from each animal. Aversive shocks (1 s, 2.00 mA DC) were generated by a stimulus isolator (ISO-Flex, A.M.P.I.) and applied through a pair of electrodes located on the skin of the face. Timing of shock presentations were synchronized with image acquisition by TTLs generated by the Prairie View software.

Chemogenetic manipulations and behavioural testing

Ligand injections: FoxP2-IRES-Cre mice and Cre-negative littermate controls were injected with a Cre-dependent AAV, as described above, and both groups were administered salvinorin B (SalB) or clozapine-N-oxide (CNO) to control for potential behavioural effects of the compounds per se. To activate KORD, mice were subcutaneously injected with 10 mg/kg SalB (catalogue # 11488; Cayman Chemical Company, Ann Arbor, MI, USA) 20 min before the behavioural testing. SalB was dissolved in DMSO at a 1 μl/g body weight injection volume using a 50 μl Hamilton Syringe (Hamilton Company, Reno, NV, USA). To activate hM3Dq, mice were injected intraperitoneally (i.p.) with 3 mg/kg CNO (catalogue # C0832–5MG; Sigma Aldrich) 30 min before the behavioural testing. CNO was dissolved in 10% DMSO in saline and injected at a volume of 10 μl/g body weight.

Fear conditioning and extinction paradigm: Behavioural tests started at 3.5 to 6 weeks after virus delivery. We did not find systematic relationship between the period between surgery and the effects of KORD both in vivo and ex vivo. Prior to testing, each mouse was handled for 2 min per day for 6 days and habituated to subcutaneous (for KORD) or intraperitoneal (for CNO) saline injections for 3 days. Fear conditioning was conducted in a 30 × 25 × 25 cm operant chamber (Med Associates, Inc., Fairfax, VT USA) with metal walls and a metal rod floor. To provide an additional olfactory cue, the chamber was cleaned between subjects with a 79.5% water/19.5% ethanol/1% vanilla extract solution. Following a 3-min baseline period, 3 pairings (60–90 s ITI) of CS (30 s, 80-dB white noise) and US (2 s 0.6 mA, co-terminating with the CS) were presented, followed by a 120-s stimulus-free period. The Med Associates Freeze Monitor system controlled CS and US presentation. Extinction training was conducted the following day (Day2) in a 27 × 27 × 14 cm operant chamber with transparent walls and a floor covered with wood chips, cleaned between subjects with a 99% water/1% acetic acid solution and housed in a different room from training. After a 3 min baseline period, either 50 (‘full extinction’) or 10 (‘partial extinction’) CSs were presented (5 s ITI)[48]. Extinction memory retrieval was tested the next day (Day3) in the same context as extinction training with 5 CS presentations (5 s inter-CS interval), following a 3-min baseline period.

Post-behaviour examination of virus expression: To examine virus expression at the completion of behavioural tests, mice were terminally overdosed with pentobarbital and transcardially perfused with PBS followed by 4% PFA in PBS. Brains were post-fixed over night at 4°C and subsequently stored in 0.1 M phosphate buffer for 1–2 days at 4°C. Coronal sections (50 μm) were cut with a vibratome (Classic 1000 model, Vibratome, Bannockburn, IL, USA). Brain sections were incubated in 1% sodium borohydride followed by blocking solution (10% normal goat serum (Vector Laboratories) and 2% bovine serum albumin (MP Biomedicals, Santa Ana, CA, USA) in 0.05 M PBS with 0.2% Triton X-100) for 2 h at room temperature (20°C), then incubated at 4°C overnight in a cocktail of primary antibodies: 1) chicken anti-GFP (1:2000 dilution, Abcam cat#13970) to aid visualization of KORD, 2) Living Colors® DsRed Polyclonal Antibody (1:1000 dilution, Clontech Labs cat# 632496) to aid visualization of hM3Dq, and 3) rabbit anti-FoxP2 (1:2000 dilution, Abcam cat#16046) to visualize ITC. The next day, sections were incubated in a cocktail of secondary antibodies: Alexa 488 goat anti-chicken IgG (1:1000 dilution, Abcam

cat#150169) and goat anti-rabbit Alexa 555 IgG (1:1000 dilution, Abcam cat# A21428). Sections were mounted and coverslipped with Vectashield HardSet mounting medium with DAPI (Vector Laboratories, Inc., Burlingame, CA, USA). Sections were imaged with an Olympus BX41 microscope (Olympus, Center Valley, PA, USA) and a Zeiss LSM 700 confocal microscope (Carl Zeiss Microscopy, Thornwood, NY, USA).

Images from the 139 Cre+ injected mice were inspected to determine whether virus expression was evident and restricted to the ITC cluster targeted and if so, whether expression was present in one or both hemispheres. Targeting success rates (rounded to the nearest %) were as follows: ITC_{vm}-targeting: 41% (21% bilateral, 20% unilateral); ITC_{dm}-targeting: 35% (17% bilateral, 17% unilateral), dual-cluster targeting: 42% (23% bilateral, 19% unilateral). Mice with absent expression were excluded from the analysis. Mice with unilateral or bilateral expression were combined given analysis of freezing behaviour on retrieval indicated generally similar results (Supplementary Table 2).

To illustrate expression patterns, virus expression in each mouse was overlayed to a corresponding coronal atlas image[47] and expression within each binned 35 μm * 40 μm segment transformed to a numerical value (expression present =1, absent = 0). Images were then aggregated across mice included in the final behavioural analysis (separately for ITC_{vm}-targeted, ITC_{dm}-targeted and dual-cluster targeted) to generate a population heatmap of expression indicating the fraction of animals exhibiting expression at each binned segment (0: no mice expressed; 1: all mice expressed) (see Extended Data Fig. 8 and 9).

Ex vivo electrophysiology

KORD functionality verification and connectivity assays between ITCs: Mice were deeply anaesthetized with 3% isoflurane in oxygen and decapitated. The brain was rapidly extracted and cooled down in ice-cold slicing artificial cerebrospinal fluid (ACSF) containing (in mM): 124 NaCl, 2.7 KCl, 26 NaH_2CO_3, 1.25 NaH_2PO_4, 10 $MgSO_4$, 2 $CaCl_2$, 18 D-Glucose, 4 ascorbic acid, equilibrated with carbogen (95% O_2 / 5% CO_2). Coronal brain slices (320 μm) containing the amygdala were cut in ice-cold slicing ACSF with a sapphire blade (Delaware Diamond Knives) on a vibrating microtome (Microm HM 650 V, Thermo Scientific). Slices were collected in a custom-built interface chamber with recording ACSF containing (in mM): 124 NaCl, 2.7 KCl, 26 NaH_2CO_3, 1.25 NaH_2PO_4, 1.3 $MgSO_4$, 2 $CaCl_2$, 18 D-Glucose, 4 ascorbic acid, equilibrated with carbogen. Slices were recovered at 37°C for 40 min and stored at room temperature. Whole-cell patch-clamp recordings were performed in a submersion chamber under an upright microscope (Olympus BX51WI), where slices were superfused with recording ACSF at 31°C. Recordings were performed using an Axon Instruments Multiclamp 700B amplifier and a Digidata 1440A digitizer (Molecular Devices). Glass micropipettes (6–8 MΩ resistance) were pulled from borosilicate capillaries (ID 0.86 mm, OD 1.5 mm, Science Products, Germany).

For KORD functionality verification the resting membrane potential and spikes were recorded in current-clamp mode with K-Gluconate based internal solution containing (in mM): 130 K-Gluconate, 5 KCl, 4 Mg-ATP, 0.4 Na-GTP, 10 Na2-phosphocreatine, 10 HEPES, 0.6 EGTA (290–295 mOsm, pH 7.2–7.3). Signals were low-pass filtered at 10

kHz and digitized at 20 kHz. Salvinorin B (Tocris Bioscience) was prepared as 1mM stock solution in DMSO, diluted to 100nM in ACSF on the day of recording, and perfused via the bath. Data from ITC_{dm} and ITC_{vm} cells were pooled for analysis.

For connectivity assays between ITC clusters, post synaptic currents were recorded in voltage-clamp configuration with cesium-based internal solution containing (in mM): 115 Cs-methanesulphonate, 20 CsCl, 4 Mg-ATP, 0.4 Na-GTP, 10 Na_2-phosphocreatine, 10 HEPES, 0.6 EGTA (290–295 mOsm, pH 7.2–7.3). Signals were low-pass filtered at 2 kHz (4-pole Bessel) and digitized at 10 kHz. Series resistance was monitored and data rejected if it changed > 25% over the course of an experiment. ChR2 was stimulated with 470 nm light pulses (0.5–1 ms duration) delivered by an LED (CoolLED *p*E) through the microscope's submersion objective (Olympus LUMPlanFL 60x, 1.0 NA). By restricting the light path aperture, illumination was confined to a small spot within the slice (80 μm diameter). Drugs were prepared from frozen stocks, diluted in ACSF and applied via superfusion for pharmacological experiments. Picrotoxin (PTX, 100 μM, Sigma, Germany) was used to block GABAergic transmission, tetrodotoxin (TTX, 1 μM, Biotrend, Germany) was first applied alone, and subsequently together with 4-aminopyridine (4-AP, 100 μM, Tocris Bioscience) to assess monosynapticity of evoked postsynaptic currents[49]. In most experiments with on-cluster stimulation, 20 μM DNQX (Biotrend, Germany) was added to the recording ACSF to block fast glutamatergic transmission.

Connectivity assays from ITCs to BLA: Mice were deeply anaesthetized (ketamine 250 mg/kg and medetomidine 2.5 mg/kg bodyweight, injected intraperitoneally) and transcardially perfused with ice-cold (0–2°C) NMDG-based solution[50,51] (in mM: 2.5 KCl, 1.25 NaH_2PO_4 (1 H_2O), 10 $MgSO_4$ (7 H_2O), 0.5 $CaCl_2$ (2 H_2O), 30 $NaHCO_3$, 20 HEPES, 25 Glucose, 93 NMDG,5 Sodium Ascorbate, 2 Thiourea, 3 Sodium Pyruvate, 93 HCl, oxygenated with 95% O_2/5% CO_2, pH 7.3–4) for 3 min. The brain was rapidly removed from the skull, and coronal brain slices (300 μm) containing ITCs and BLA were prepared in ice-cold NMDG-based solution with a vibrating-blade microtome (HM650V, Microm) equipped with a sapphire blade (Delaware Diamond Knives). For recovery, slices were kept in the dark for 10 min at 33°C in an interface chamber containing the NMDG-based solution and afterwards at room temperature (20–24°C) in Hepes-holding solution (in mM: 20 HEPES, 92 NaCl, 2.5 KCl, 1.25 NaH_2PO_4 (1 H_2O), 2 $MgSO_4$ (7 H_2O), 2 $CaCl_2$ (2 H_2O), 25 Glucose, 30 $NaHCO_3$, 5 Sodium Ascorbate, 2 Thiourea, 3 Sodium Pyruvate, oxygenated with 95% O_2/5% CO_2, pH 7.4) for at least 1 h until recording.

Experiments were performed in a submerged chamber on an upright microscope (BX50WI, Olympus) superfused with oxygenated recording ACSF (in mM: 123 NaCl, 3 KCl, 1.25 NaH_2PO_4 (1 H_2O), 1 $MgCl_2$ (6 H_2O), 2 $CaCl_2$ (2 H_2O), 11 Glucose, 26 $NaHCO_3$, 10 μM CNQX and 10 μM CPP) at a perfusion rate of 4 ml/min at 32°C. $EGFP^+$ ITC clusters and CTB^+ BLA projection neurons were visualized using epifluorescence and a 5x air immersion objective(LMPlanFI 5x/0.15 NA, Olympus) or a 40x water immersion objective (LumPlanFl 40x/0.8 NA, Olympus). Patch electrodes (for BLA, 3–5 MΩ; for ITCs, 7–8 MΩ;) were pulled from borosilicate glass tubing and filled with internal solution (for voltage-clamp recordings in mM: 110 CsCl, 30 K-gluconate, 1.1 EGTA, 10 HEPES, 0.1 $CaCl_2$, 4 Mg-ATP, 0.3 Na-GTP, 4 QX-314 chloride, pH 7.3; for current-clamp recordings

in mM: 130 K-methylsulfate, 10 HEPES, 10 Na-phosphocreatine, 4 Mg-ATP, 0.3 Na-GTP, 5 KCl, 0.6 EGTA, pH 7.3). In some experiments, 0.4% biocytin was added to post-hoc visualize recorded neurons. Voltage-clamp recordings from BLA neurons were acquired in whole-cell mode at a holding potential of −70 mV. soCoChR expressing ITC_{dm} and ITC_{vm} were photostimulated using blue LEDs (PlexBright Blue, 465 nm, with LED-driver LD-1, Plexon) connected to optical fibres (0.39NA, FT200EMT, Thorlabs) positioned above them. Five blue light pulses of 0.6 mW (at the fibre-tip) with 10-ms duration were applied at a frequency of 0.5 Hz. Inhibitory postsynaptic currents were averaged across at least 10 light pulses. In some slices, PTX (100 μM) was administered with the recording ACSF for the last cell recorded from. In current-clamp recordings from ITCs, spikes were evoked from a holding potential of about −70 mV with the same blue light stimulation protocol as above. Data was acquired with a Multiclamp 700B amplifier, Digidata 1440A A/D converter and pClamp 10 software (all Molecular Devices) at 20 kHz and filtered at 10 kHz. Data were excluded if the access resistance exceeded 25 MΩ or 10% of the membrane resistance or changed more than 20% during the recordings. All chemicals were purchased from Sigma-Aldrich except for CNQX, CPP and QX-314 (Tocris Bioscience).

Post-hoc histological analysis for connectivity assays between ITCs: Following recordings, slices were sandwiched between two cellulose nitrate filter papers (0.45 μm pore size, Sartorius, Germany) and fixed in 4% PFA in 0.1 M phosphate buffered saline (PBS, pH 7.4) overnight. To confirm cluster-specific ChR2-EYFP expression, fixed slices were re-sectioned at 60 μm thickness with a vibrating microtome (Microm HM 650 V, Thermo Scientific). Free floating sections were incubated in blocking solution (20% horse serum, 0.03% Triton X-100 in PBS) for 2 h at room temperature, and then overnight in PBS with 10% blocking solution and primary antibodies at a 1:1000 dilution; in all cases against EYFP fused to channelrhodopsin2 (Goat- anti-GFP polyclonal), in some batches also against FoxP2 (Rabbit- anti-FoxP2 polyclonal). On the next day, sections were washed 3 times for 10 min in PBS, and incubated for 2 h at room temperature in PBS with 10% blocking solution and secondary antibodies at 1:1000 dilution; in all cases with Donkey-anti-goat-Alexa488, for FoxP2 staining additionally with Donkey-anti-rabbit-Alexa555. Slices were then washed 3 times for 10 minutes in PBS, incubated for 25 min in 1:500 Neurotrace 435/455 in PBS, and washed 3 more times for 10 minutes in PBS. Sections were then mounted on glass slides in mounting medium (Vectashield, Vector Laboratories) and imaged with a confocal microscope (LSM 710, Zeiss).

Fibre photometry recording

A modified Doric Fibre Photometry system was used to perform the recordings. Three different excitation wavelengths were used (465 nm for Ca^{2+}-dependent jGCaMP7f activity, 560 nm for Ca^{2+}-dependent jRGECO1a activity, and 405 nm to record an isosbestic, Ca^{2+}-independent, reference signal that serves to correct for photo-bleaching and movement-related artifacts[52]. The light intensity used for each wavelength was < 100 μW at the fibre tip. Optical patch cables were extensively photo-bleached before recordings to reduce auto-fluorescence and a lock-in modulation/demodulation procedure was used to improve the signal-to-noise ratio and spectral separation of the fluorescent signals[53]. Data were digitized and recorded at 20 kHz.

Elevated zero-maze paradigm: The elevated zero-maze with a 55 diameter and a 5 cm width corridor was composed of two open and two closed quadrants, which are equivalent to 90° each, elevated at 50 cm above the ground. Two external walls and two internal walls with 15 cm height for the closed quadrants were made of opaque plastic and transparent plexiglass, respectively. Mice were allowed to freely explore the maze for 15 min. Mouse behaviours were video recorded with a camera controlled with a custom written code in Bonsai[54], while synchronized with photometry recording via TTL pulses. The videos were post-hoc analysed by a second custom written code in Bonsai and the position of the mouse in the open versus closed quadrants determined as the central position of the body mass.

Quantification and statistical analysis

Analysis of behaviour during calcium imaging: All behavioural sessions were recorded using an overhead camera (Stingray, Allied Vision) and Cineplex software (Plexon) at 40 Hz. Mice were tracked using contour tracking, and freezing behaviour was automatically scored with the assistance of a frame-by-frame analysis of pixel change (Cineplex Editor, Plexon). Freezing behaviour minimum duration threshold was set to 2 s. Automatically detected freezing epochs were manually inspected on the video recording to eliminate false-positive and false-negative freezing bouts (e.g., during micro-grooming episodes or due to motion artefacts caused by cable movement, respectively). Annotated freezing data were then temporally aligned with miniscope imaged data and finally downsampled to 10 Hz.

Analysis of behaviour for chemogenetic manipulation: Behavioural sessions were video recorded with The Med Associates Freeze Monitor system (fear conditioning) or with GoPro HERO7 video camera (extinction training and retrieval). Based on the recorded videos, freezing was manually scored at 5 s intervals throughout testing by an experienced observer blind to genotype. The mean numbers of freezing observations per baseline period and 5x CS blocks were converted to a percentage [(number of freezing observations/total number of observations per period) × 100] for analysis. Mice with freezing scores on any CS-block >3 standard deviations from the group mean were excluded from the analysis.

Analysis of miniature microscope calcium imaging data: Imaging frames were down-sampled to 540 × 540 pixels at 10 Hz and normalized across the whole frame by dividing each frame by a Fast Fourier Transform band pass-filtered version of the frame using ImageJ (NIH)[19]. Motion artifact correction and PCA/ICA-based cell detection was performed with MosaicAPI (Inscopix) for MATLAB. Edges of cell masks were then smoothed by open/close functions. Raw calcium traces were obtained by averaging all the pixel values in each mask. Slow drift of the baseline signal over the course of minutes was removed using a low-cut filter (Gaussian, cutoff, 2 – 4 min). Relative changes in calcium fluorescence F were calculated by $\Delta F/F0 = (F - F0)/F0$ (with F0 = median fluorescence of entire trace). When a cell pair showed (1) distance between centroids < 15 pixels (2) correlation coefficient between entire time courses > 0.6, one of the pair was manually eliminated to avoid double-counting. Finally, pairs of the mask and the trace of all the cells were manually inspected to exclude false-positive/negative cell mask allocation. For fear extinction, images from consecutive 5 days were concatenated before the motion correction

procedure. When there was major displacement of the field of view (FOV) and same set of neurons were not able to be identified across days, animals were excluded.

To define responsive cells, trial-averaged Ca^{2+} signals were compared between the stimulus and a temporally equivalent baseline period using a Wilcoxon rank-sum test with a significance threshold of $P < 0.05$. The windows for averaging were 2 s (shock), 4 s (CS-offset), and 29 s (CS), from stimulus-onset. AUC (area under the curve) ΔF/F values were calculated using these same windows. A cell was classified as a fear neuron if it exhibited a significant tone response after fear conditioning (CS 1–5 during Ext1 (Day3), when freezing levels were highest), but no significant response after extinction (CS 21–25 during Ext2 (Day4), when freezing levels were lowest), and vice versa for extinction neurons. Finally, units were classified as extinction-resistant neurons if they displayed a significant tone response during both time points[23,55,56].

Analysis of 2-photon calcium imaging data: The images were analysed by using custom written in-house software running on MATLAB (Mathworks). First, acquired images were motion corrected with NoRMCorre[57]. Artifacts caused by bi-directional scanning were corrected by shifting odd lines and even lines. Cell outlines were manually identified using ROI-manager function in ImageJ, based on motion corrected movies and maximum intensity projections. Time courses of individual cells were extracted by summing the pixel values within the cell outlines. Slow drift of the baseline signal over the course of minutes was removed using a low-cut filter (Gaussian, cutoff, 2–4 min). Raw calcium signal time courses were corrected to minimize out-of-focus signal contamination: neuropil signals were subtracted from cell body signals after multiplying by a fixed contamination ratio: 0.7 as previously described[58,59].

Analysis of fibre photometry recordings: Analysis was performed with custom programs written in MATLAB (Mathworks). Data with obvious motion artifacts in the isosbestic channel were discarded. Demodulated raw Ca^{2+} traces were down-sampled to 1 kHz and then de-trended using a low-cut filter (Gaussian, cutoff, 2–4 min) to correct for slow drift of the baseline signal due to bleaching. Filtered traces were Z-scored by mean and standard error of the entire trace.

Analysis of slice whole-cell recordings: Data were analysed with custom written codes in Python 3.7 (Anaconda distribution) running the pyABF module, custom written Macros in IgorPro (Wavemetrics, USA), or custom programs written in MATLAB (Mathworks) using abfload (Harald Hentschke/Forrest Collman) function. Connectivity was defined by comparing signal vs baseline (10 trials), while statistical significance was assessed by Wilcoxon signed-rank test.

Statistical analyses and data presentation

All data are expressed as the mean ± standard error of the mean (SEM), unless stated otherwise. Box plots represent the median and 25th and 75th percentiles, and their whiskers represent the data range. In some of the plots, outlier values are not shown for clarity of presentation, but all data points and animals were always included in the statistical analysis.

Two-sided Wilcoxon rank-sum test was used to compare two independent groups. For paired comparison, we used Wilcoxon signed-rank test or paired t-test based on distribution and n size of the data. An ANOVA was performed when more than two groups were compared, which was followed by Tukey-Kramer post-hoc method. For multiple comparisons against a baseline, Dunnett's test was used. For comparing 2 distributions, Kolmogorov Smirnov test was applied. For trend, Jonckheere-Terpstra test was used. For categorical data, Chi-squared test or Fisher's exact test (when sample sizes and expected frequencies are small) was applied. For repeated observations of freezing scores, a repeated measures ANOVA was used, which was followed by Sidak post-hoc method. All data analyzed by ANOVA were normally distributed according to a Kolmogorov-Smirnov test on the ANOVA residuals. Throughout the study, $P < 0.05$ was considered statistically significant. No statistical methods were used to pre-determine sample sizes, but our sample sizes are similar to those generally employed in the field.

Data availability

The data that support the findings of this study are available at: https://data.fmi.ch/PublicationSupplementRepo/

Code availability

Custom-written codes used to analyse data from this study are available upon reasonable request from the corresponding authors.

Extended Data

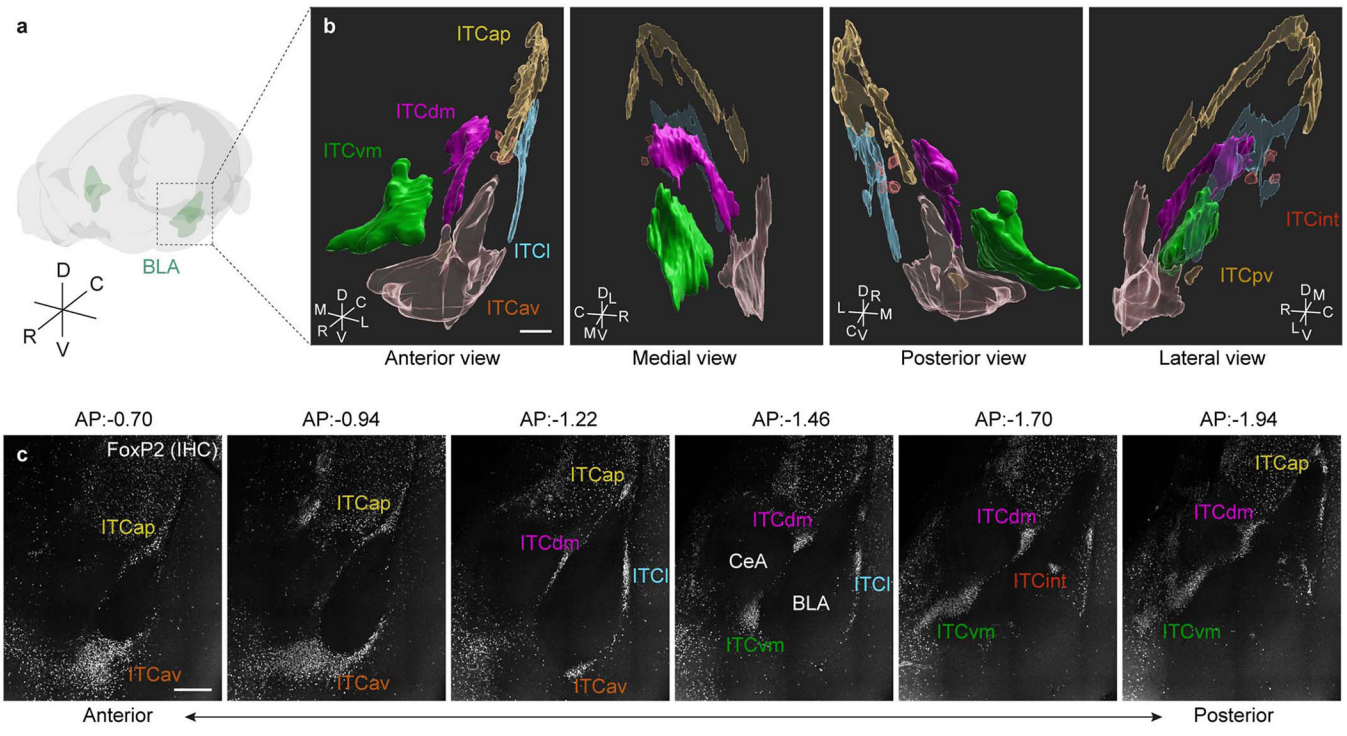

Extended Data Fig. 1 |. 3D-reconstruction of individual ITC clusters

a, Schematic of a mouse brain volume. R: Rostral; C: Caudal; D: Dorsal; V: Ventral.
b, 3D reconstructions were separately obtained via 1) anti-FoxP2 immunostaining, 2) a FoxP2-Cre x Ai14 mouse, and 3) D1R-Cre x Ai14 mouse, in triplicate for each method. ITC_{ap}: apical; ITC_{dm}: dorsomedial; ITC_{vm}: ventromedial; ITC_{l}: lateral; ITC_{av}: anteroventral; ITC_{int}: internal; ITC_{pv}: posteroventral R: Rostral; C: Caudal; D: Dorsal; V: Ventral; M: Medial; L: Lateral; Scale bar: 300 μm.
c, Example planes of a cleared 3D-tissue obtained from a WT mouse stained with an anti-FoxP2 antibody covering the anterior-posterior axis of ITC clusters. Bregma levels are indicated above each panel. Scale bar: 300 μm.
See also Supplementary Movie 1 and Table 1.

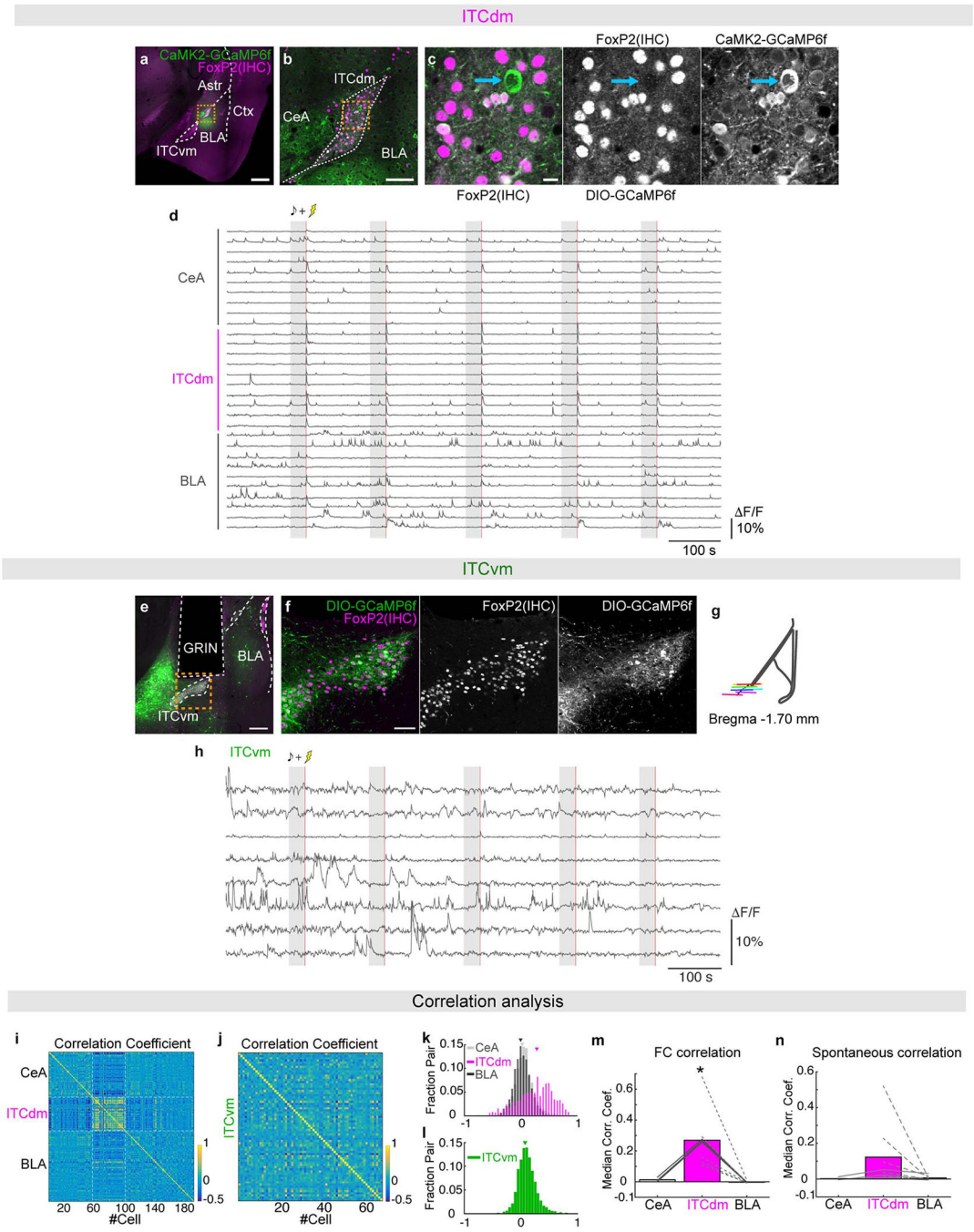

Extended Data Fig. 2 |. Ca^{2+} imaging from ITC_{dm} and ITC_{vm}.

a-c, Histological validation of GCaMP6f expression. Wild-type mice (not used for *in vivo* imaging) (N = 2) were injected with an AAV-CaMK2-GCaMP6f and sacrificed after 1 month of expression. Thin slices (120 μm) were cut and stained with an anti-FoxP2 antibody. In addition to BLA and CeA neurons, most of the FoxP2-positive ITC_{dm} neurons expressed GCaMP6f. Blue arrow shows a putative large, FoxP2-negative ITC neuron. Scale bars: 500 μm (**a**), 100 μm (**b**), and 10 μm (**c**).

d, Example Ca^{2+} traces from simultaneously imaged neurons in the CeA, ITC_{dm}, and BLA with a miniature microscope during fear conditioning. Data obtained from the same mice as shown in Fig. 1d–g. Gray shading indicates CS presentation (30 s); red line indicates footshock US presentations (1 s).

e,f, Histological validation of GCaMP6f expression in ITC_{vm} neurons. FoxP2-Cre mice were injected with an AAV encoding Cre-dependent GCaMP6f, implanted with a GRIN lens, and sacrificed after behavioural experiments. Thin slices (120 μm) were cut and stained with an anti-FoxP2 antibody. Scale bars: 200 μm (**e**), 50 μm (**f**). Similar results were obtained with all the six mice.

g, Summary of histologically confirmed GRIN lens implantation locations for ITC_{vm} recordings. Animals with off-target implantations were excluded from analysis.

h, Example Ca^{2+} traces from neurons in the ITC_{vm} cluster during fear conditioning. Gray shading indicates CS presentation (30 s); red line indicates footshock US presentations (1s). Images of GCaMP6f expression from the same mouse are shown in panel **e,f**.

i,j, Correlation matrices of all simultaneously-recorded neuron pairs in CeA, ITC_{dm}, and BLA (**i**), or in ITC_{vm} (**j**) from representative animals. The entire recording session (11 min) was used.

k, Distributions of correlation coefficients from CeA/CeA, ITC_{dm}/ITC_{dm}, and BLA/BLA pairs. Arrows indicate median of the distributions.

l, Distribution of correlation coefficients from ITC_{vm}/ITC_{vm} pairs. Arrow indicates median of the distribution.

m, Summary of medians of correlation coefficient distribution shown in **(k)**. Solid lines indicate individual animals in which CeA, the ITC_{dm} cluster, and BLA were simultaneously imaged (N = 3). Dotted lines indicate animals in which only the ITC_{dm} cluster and BLA were simultaneously imaged (N = 5). * $P = 0.007$, one-way ANOVA followed by Tukey-Kramer.

n, Medians of correlation coefficient distribution. The same analysis as **(m)** was applied to data from home-cage recording sessions. ITC_{dm} neurons also shows a trend towards a higher correlation in the absence of CS or US stimulation. * $P = 0.12$, one-way ANOVA.

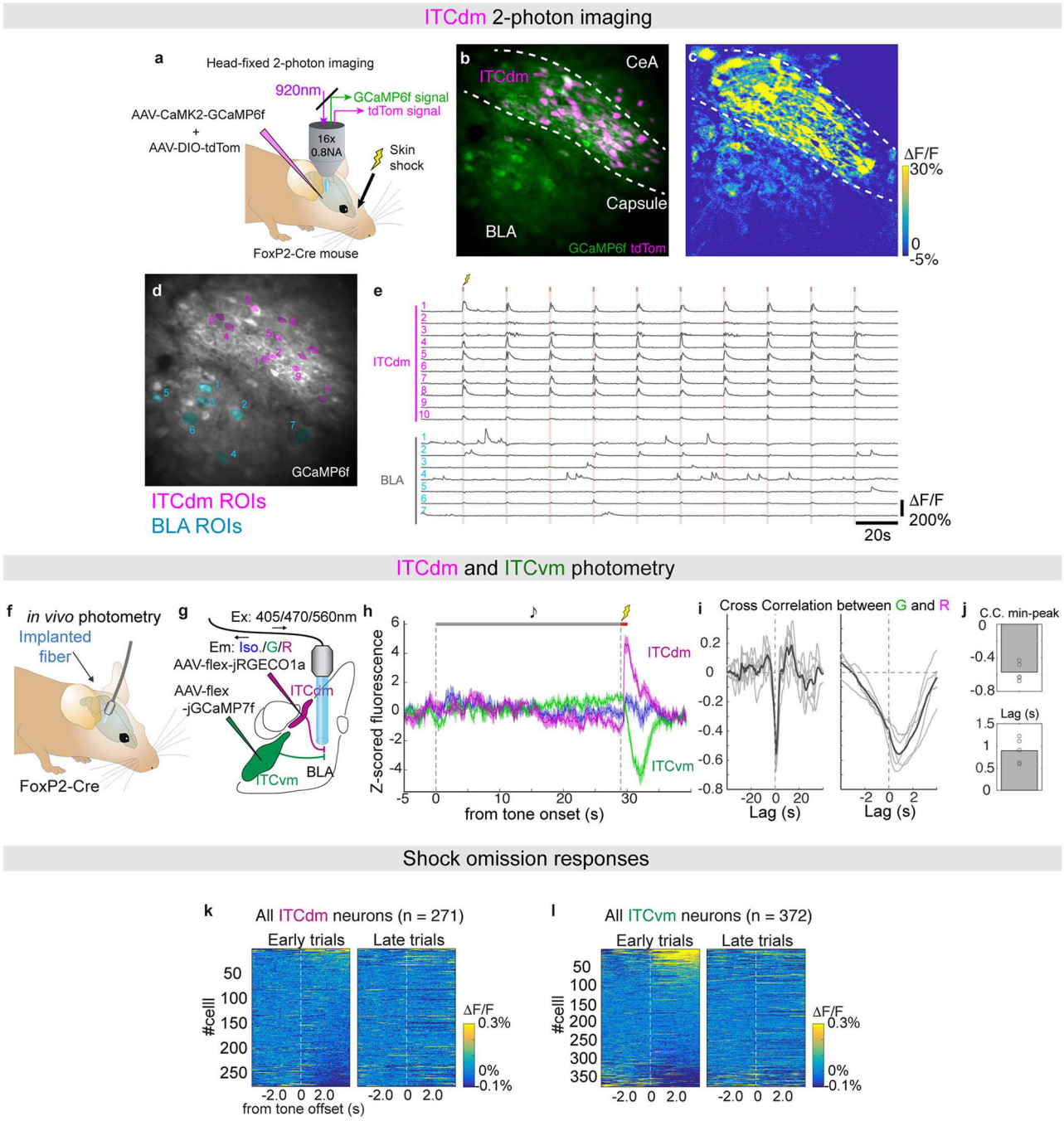

Extended Data Fig. 3 |. 2-photon imaging and fibre photometry.

a, Schematic showing dual-colour *in vivo* 2-photon imaging through the implanted GRIN lens. ITC_{dm} neurons were labelled by co-injection of an AAV expressing Cre-dependent tdTomato in FoxP2-Cre mice. A GRIN lens was implanted above ITC_{dm} and surrounding BLA and CeA to record Ca^{2+} responses to aversive skin shocks (USs).

b, Mean projected FOV. Green: GCaMP6; Magenta: tdTomato. The dashed lines indicate the intermediate capsule surrounding ITC_{dm}.

c, Heatplot of Ca^{2+} responses (ΔF/F) to US presentations showing clustered activation of ITC_{dm} neurons.

d, ROIs corresponding to ITC_{dm} (Magenta) and BLA (Blue) neurons. ROI numbers correspond to traces shown in **e**.

e, Example Ca^{2+} traces from ITC_{dm} and BLA neurons. Red lines indicate US presentations (1 s). Note, we confirmed that face skin shock used in this experiment and footshock similarly activated ITC_{dm} neurons (data not shown).

f, Schematic illustrating *in vivo* fibre photometry in a freely-moving mouse.

g, ITC_{dm} and ITC_{vm} clusters were targeted with AAVs encoding Cre-dependent jRGECO1a or jGCaMP7f, respectively. Recording fibres were placed in BLA to simultaneously monitor axon terminal Ca^{2+} dynamics of ITC_{dm} and ITC_{vm} axons. Isosbestic control signals were recorded in the blue channel.

h, Example traces of simultaneously recorded dual-colour Ca^{2+} signals and a control signal during a fear conditioning session.

i, Cross correlation traces between two simultaneously recorded Ca^{2+} signals. Dark gray lines represent 5-trial averaged traces and light gray lines represent individual trials.

j, (*Top*) Minimum peak values of cross correlation. (*Bottom*) Lags of the minimum peak points. (N = 2 mice)

k,l, Activity heatplot of trial-averaged responses (*Left*: first 5 trials, *Right*: last 5 trials) to footshock US omissions of all the recorded ITC_{dm} (n = 271 neurons, from 9 mice) (**k**) or ITC_{vm} neurons (n = 372 neurons, from 6 mice) (**l**) aligned by CS offset. Cells were sorted based on their averaged ΔF/F responses in the first 5 trials.

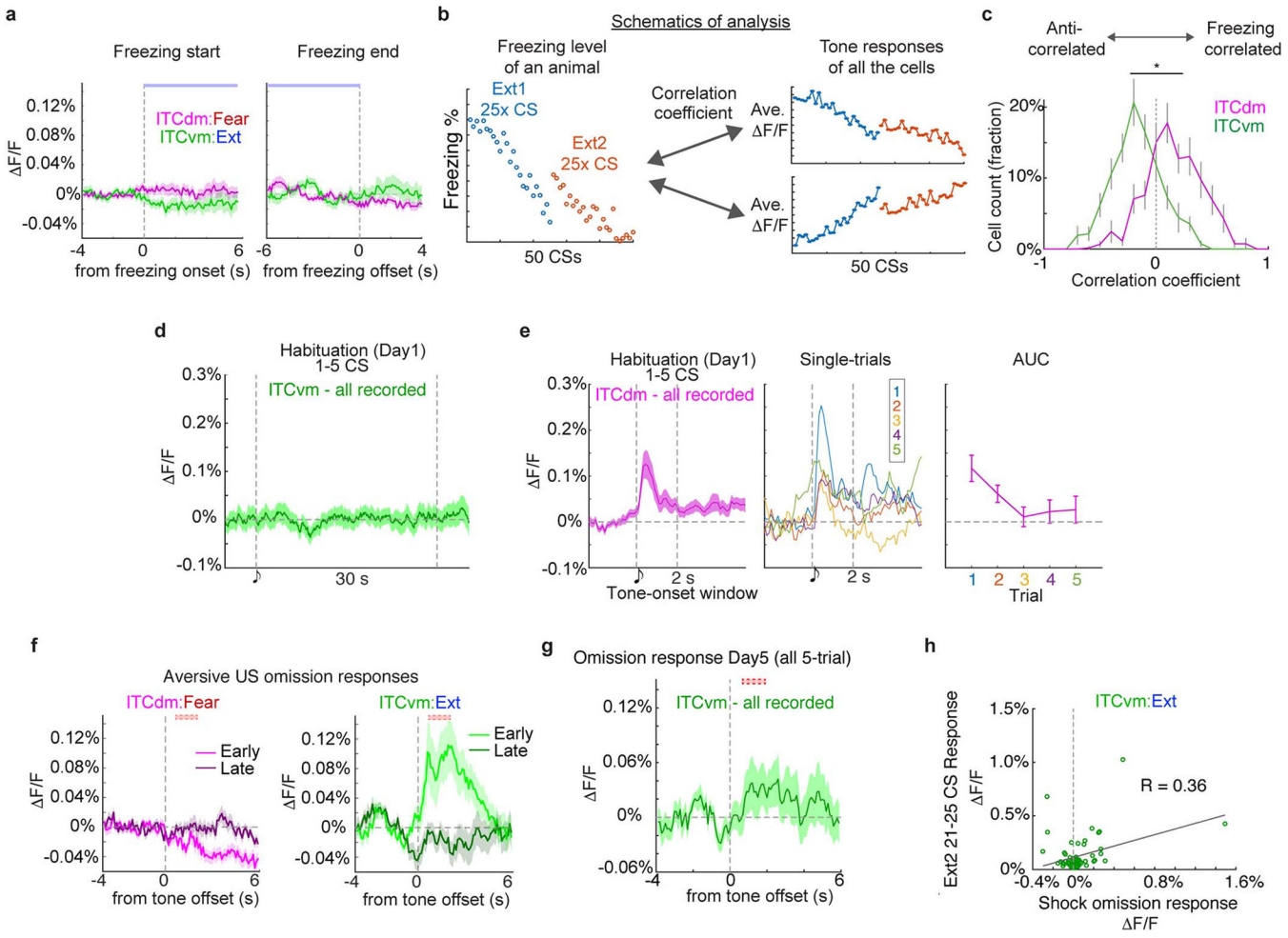

Extended Data Fig. 4 |. Population activity of ITC_{dm} and ITC_{vm} neurons.

a,b, Heatplots of all recorded neurons. (**a**) 271 ITC_{dm} neurons from 9 mice and (**b**) 372 ITC_{vm} neurons from 6 mice throughout the entire 5-day fear conditioning/extinction paradigm. Neurons were sorted by their classification into Fear, Extinction, Extinction Resistant, and non-Responsive neurons.

c, Example Ca^{2+} traces of a Fear and Extinction neuron from ITC_{dm} and ITC_{vm}, respectively for all time points indicate shown in panels **(a,b)**. Habituation, Ext1: 1–5, Ext2: 21–25, and Retrieval time points are duplicated in Fig. 2c.

d, Scatter plots visualising distributions of tone responses of all the recorded ITC_{dm} neurons (Left) and ITC_{vm} neurons (Middle and Right) during Ext1: 1–5 and Ext 2: 21–25 trials. Functional cell-types – Fear, Extinction, and Extinction Resistant neurons – are plotted with different colours, non-responsive neurons in grey (c.f. Fig. 2d).

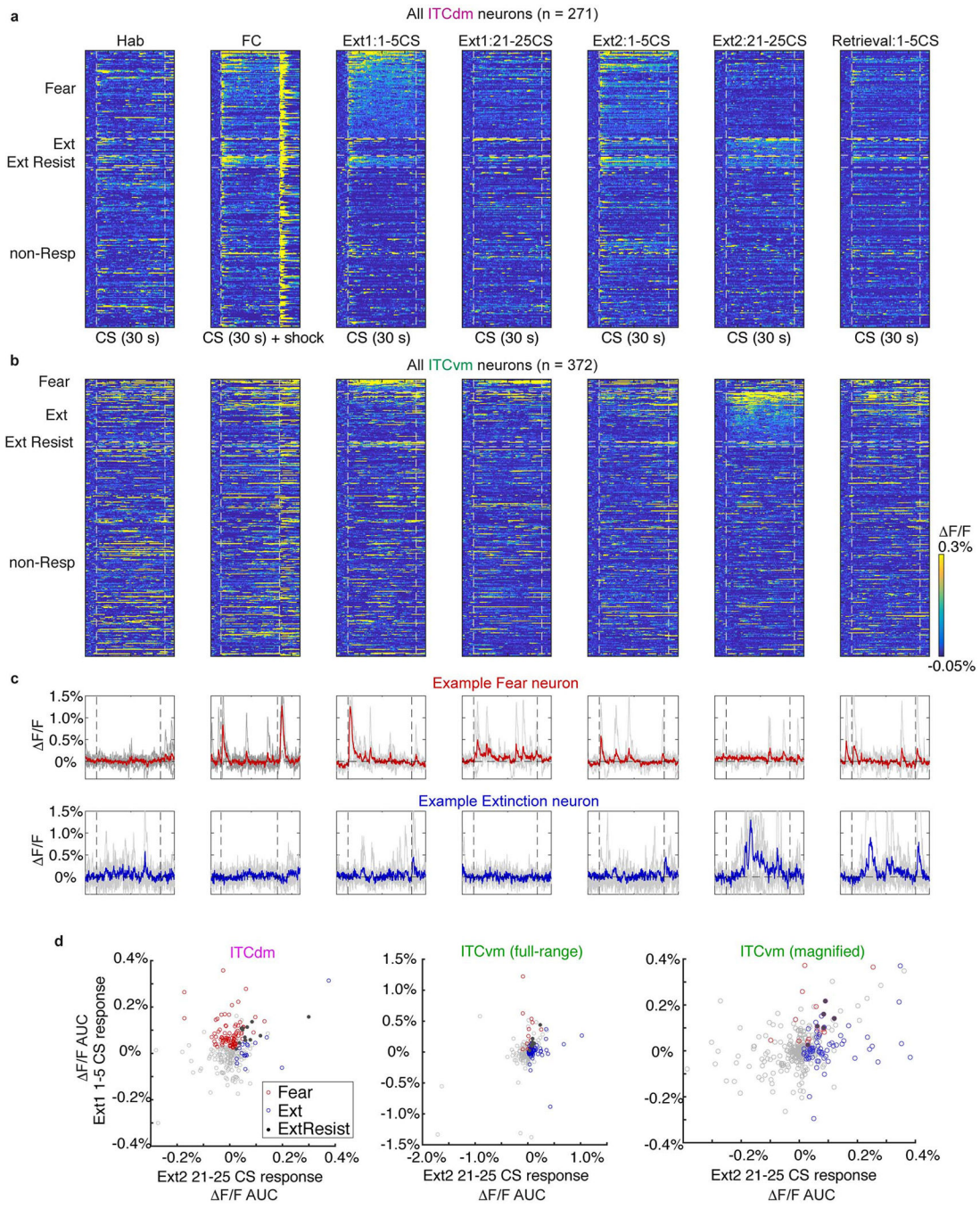

Extended Data Fig. 5 |. Properties of ITC_{dm} and ITC_{vm} neurons during fear extinction.

a, Trial-averaged ΔF/F Ca^{2+} responses of ITC_{dm} Fear and ITC_{vm} Extinction neurons aligned to freezing onset and offset.

b, Schematics illustrating the analysis shown in (**c**). Correlation coefficients between trial-by-trial (in total, 50 CS trials) freezing levels and CS-response amplitudes of all the recorded neurons across two days of extinction. Distribution of those correlation coefficients (one value from each neuron) were first normalized in each animal, then mean ± SEM values were acquired from all ITC_{dm} and ITC_{vm} recordings and visualized.

c, The distribution of correlation coefficients for ITC_{dm} neurons was skewed towards 1, indicating a larger fraction showed a CS response pattern positively correlated with freezing behaviour. In contrast, ITC_{vm} neurons exhibited the opposite tendency; a response pattern anti-correlated with freezing behaviour. $*P = 1.64 \times 10^{-40}$, Kolmogorov–Smirnov test.
d, Trial-averaged ΔF/F Ca^{2+} responses of ITC_{vm} neurons aligned to tone on habituation (Day1).
e, (*Left*) Averaged Ca^{2+} responses to tone CS onset of ITC_{dm}. Vertical dotted lines indicate onsets and 2 seconds time-window of CSs for AUC analysis. (*Center*) Single-trial average of all the ITC_{dm} neurons. (Right) Area under the curve (AUC) quantification of single-trial responses shown in the *Center* panel. $P = 0.027$, one-way ANOVA.
f, Trial-averaged ΔF/F Ca^{2+} responses of ITC_{dm} Fear and ITC_{vm} Extinction neurons aligned to US omission on Day3. Early: CS1–5, Late: CS21–25. Dotted red boxes indicate the expected timing of US delivery.
g, Trial-averaged ΔF/F Ca^{2+} responses of all recorded ITC_{vm} neurons aligned to US omission on Day5. The dotted red box indicates the expected timing of US delivery.
h, Relationship between CS responses during last 5 trials of extinction training on Day4 and US omission responses on Day3 in ITC_{vm} Extinction neurons shows a weak positive correlation.

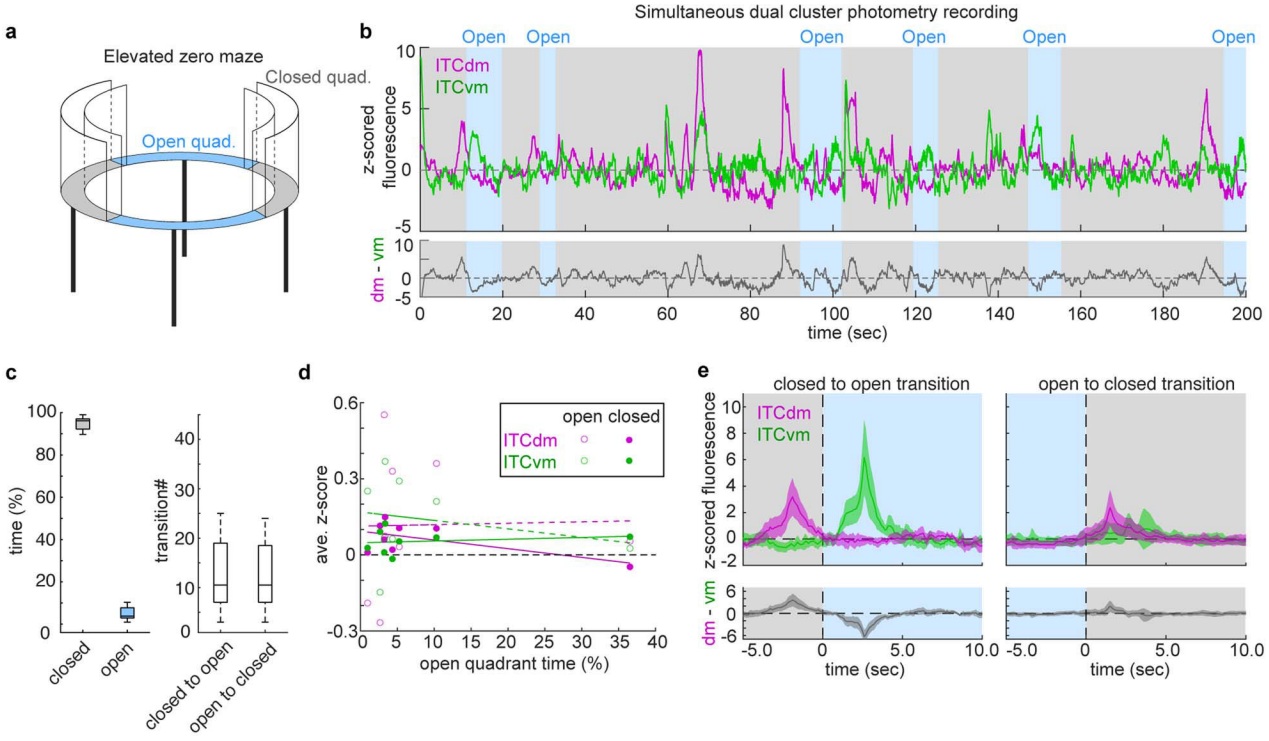

Extended Data Fig. 6 |. Simultaneous photometry recordings from ITC_{dm} and ITC_{vm} during state transition

a, Schematic of an elevated zero-maze apparatus.
b, (Top) Example z-scored Ca^{2+} traces of simultaneously recorded ITC_{dm} (magenta) and ITC_{vm} (green) neurons with the corresponding location in the maze indicated with gray

(closed quadrant) and blue (open quadrant) shading. (Bottom) Difference between the ITC_{dm} and ITC_{vm} signals.

c, (Left) Percentage of time spent in closed and open quadrants. (Right) Total number of transitions from close to open quadrants (15 ± 3.9, mean ± SEM) or from open to closed quadrants. N = 5 mice. Box plots represent the median and 25th and 75th percentiles, and their whiskers represent the data range.

d, Averaged activity of ITC_{dm} or ITC_{vm} neurons in the closed or open quadrants did not correlate with the total time spent in open quadrants. Regarding the larger variability in ITC activities in open quadrants, we note that the time an animal spent in open quadrants was, on average, much shorter than that in closed quadrants (**c**). As such, activity in open quadrants was to a lesser extent averaged out, resulting in higher variability. 8 sessions from N = 5 mice.

e, (Top) Averaged Ca^{2+} traces during transitions between quadrants. Changes in the balance between ITC_{dm} and ITC_{vm} parallel a transition from a closed to an open quadrant. (Bottom) Difference between the ITC_{dm} and ITC_{vm} signals.

Briefly stated, the results of this experiment make at least three important points: 1) the role of the ITC clusters extends beyond signaling acute, cue-triggered fear states to conditioned fear stimuli to encompass state transitions during exploration of a potentially threatening environment, 2) the clusters exhibit markedly divergent, opposing responses to transitions between protected and unprotected environments, as they do in response to conditioned and extinguished fear cues, 3) the pattern of results shows that increased ITC_{vm} activity occurs when the animal moves from the protected, closed, to the unprotected, open, quadrants. Potentially, this increase in ITC_{vm} neuron activity may serve to inhibit defensive behaviour and thereby enable exploration of the unprotected open quadrants, analogous to the inhibition of freezing behaviour following extinction. Such cross-task neuronal function is not without precedent, for example BLA neuronal activity during elevated plus-maze open arm exploration is anti-correlated with conditioned freezing behaviour in the same mice[60].

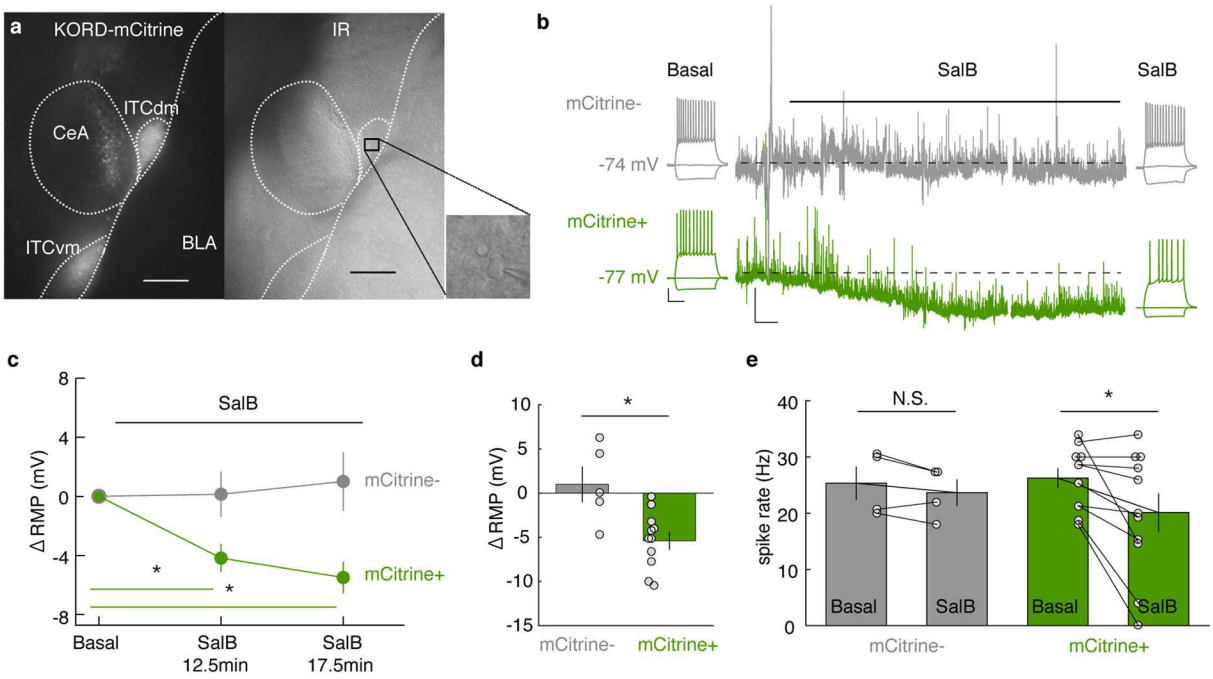

Extended Data Fig. 7 |. *Ex vivo* validation of KORD.

a, Fluorescence (mCitrine, left) and infrared (IR, right) images from a slice used for recordings in a FoxP2-Cre mouse injected with an AAV-DIO-KORD-mCitrine into ITC_{dm} and ITC_{vm}. Inset: Infrared image from a recorded ITC_{dm} neuron. Scale bar: 200 μm.

b, Representative current-clamp traces illustrating supra-threshold responses to a +60 pA current injection and continuous recording of the resting membrane potential (RMP) during application of Salvinorin B (SalB, 100 nM) from control (mCitrine−) and KORD-infected (mCitrine+) ITC neurons. Scale bars: RMP: 5 mV, 1 min; current steps: 20 mV, 200 ms.

c, SalB application induced a significant hyperpolarization of the membrane potential in mCitrine+ neurons (n = 10 neurons from 4 mice) at both time points vs. baseline (12.5-min: * $P = 0.003$, 17.5-min: * $P = 0.0001$, Two-sided Dunnett's test). Changes in membrane potential were not significant in the mCitrine− control neurons (n = 5 neurons from 3 mice) at both time points vs. baseline (12.5-min: $P = 0.99$, 17.5-min: $P = 0.84$, Dunnett's test). Error bars: mean ± SEM

d, Comparison of membrane potential changes (ΔRMP) at 17.5 min after application of SalB. Changes in KORD-infected neurons (mCitrine+) were significantly different from control (* $P = 0.013$, Wilcoxon rank-sum test; n = 5 neurons from 3 mice and n =11 neurons from 5 mice for mCitrine− and mCitrine+, respectively). Error bars: mean ± SEM

e, Comparisons of spike rates in response to +60 pA current injections before and 17.5 min after application of SalB. KORD-infected neurons (mCitrine+, n = 11) significantly reduced spike rate (from 26.2 ± 1.69 Hz to 20.1 ± 3.30 Hz, * $P = 0.016$, Wilcoxon signed-rank test). In contrast, mCitrine- neurons (n = 4 neurons from 3 mice) did not show a significant reduction in spike rate (from 25.3 ± 2.89 Hz to 23.7 ± 2.27 Hz, $P = 0.25$, Wilcoxon signed-rank test). Error bars: mean ± SEM

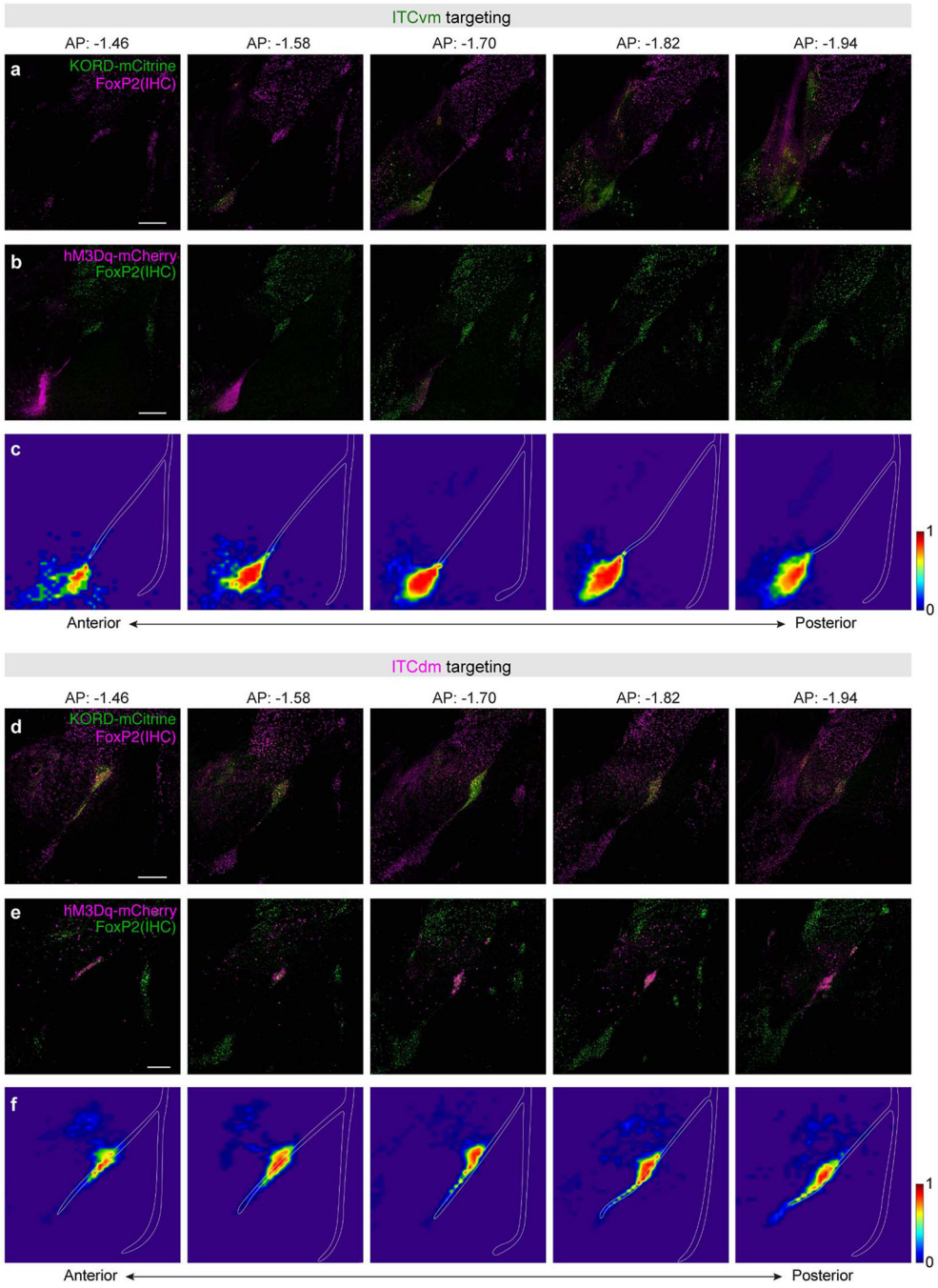

Extended Data Fig. 8 |. Histology for chemogenetic manipulations of distinct ITC clusters.
a, Examples of histological validation of KORD-mCitrine expression in ITC_{vm} neurons across multiple anterior-to-posterior coronal sections. Following all the behavioural experiments (Fig. 3), mice were sacrificed and slices (50 μm) cut and stained with an anti-FoxP2 antibody. Scale bar: 200 μm.
b, Examples of histological validation of hM3Dq-mCherry expression in ITC_{vm} neurons across multiple anterior-to-posterior coronal sections. Scale bar: 200 μm.

c, Heatmaps illustrating virus expression aggregated across Cre+ mice in **(a)** and **(b)**. Scale bar indicates the fraction of animals exhibiting expression at each locus (0: no mice expressed; 1: all mice expressed).

d, Examples of histological validation of KORD-mCitrine expression in ITC_{dm} neurons across multiple anterior-to-posterior coronal sections. Scale bar: 200 μm.

e, Examples of histological validation of hM3Dq-mCherry expression in ITC_{dm} neurons across multiple anterior-to-posterior coronal sections. Scale bar: 200 μm.

f, Heatmaps illustrating virus expression aggregated across Cre+ mice in **(d)** and **(e)**. Scale bar indicates the fraction of animals exhibiting expression at each locus (0: no mice expressed; 1: all mice expressed). Bregma levels are note above the panels in **(a)** and **(d)**.

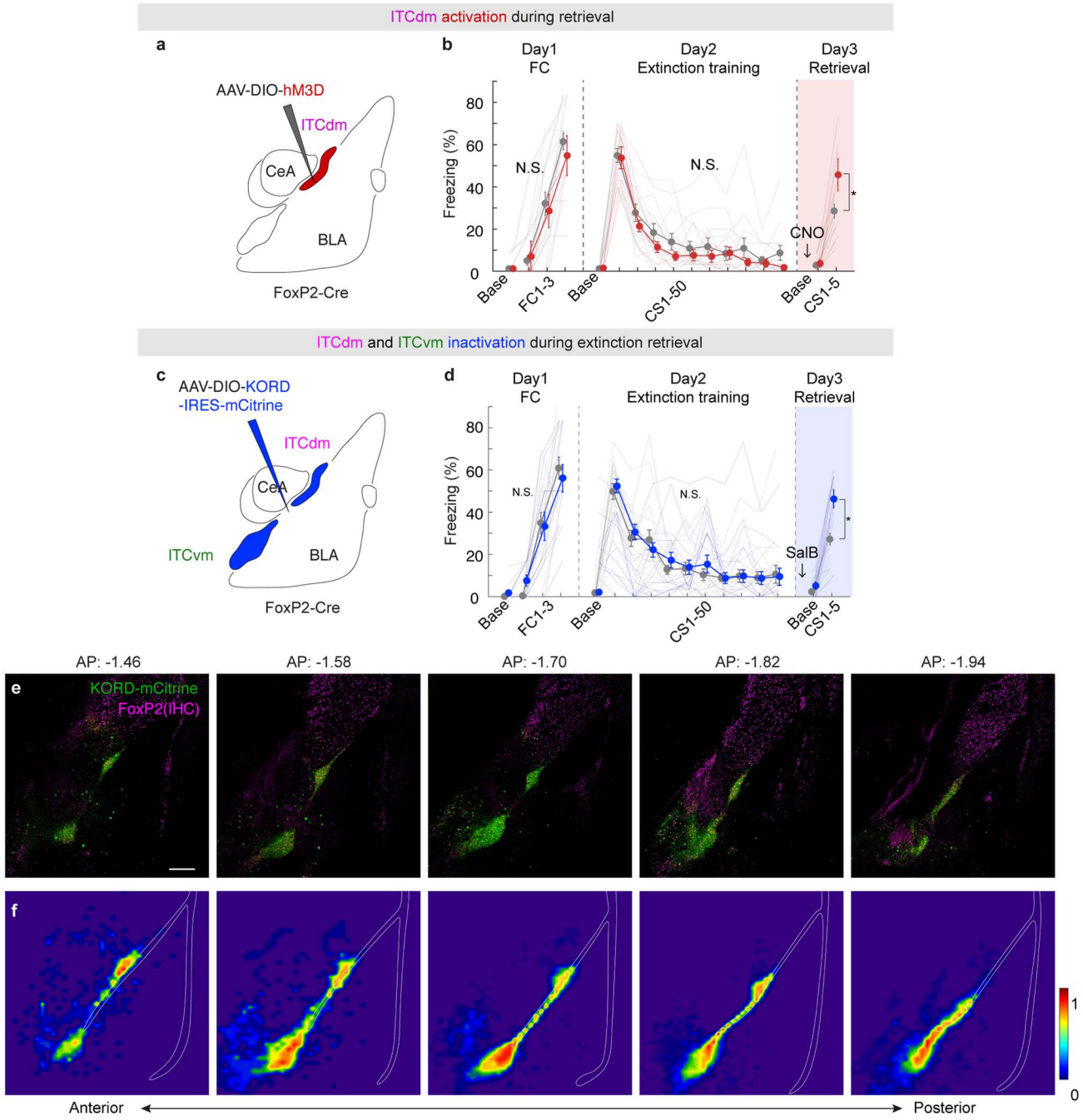

Extended Data Fig. 9. Additional chemogenetic manipulations of ITC_{dm} and ITC_{vm} clusters.

a, Chemogenetic manipulations. AAV encoding Cre-dependent hM3Dq targeted to ITC_{dm} neurons in FoxP2-Cre mice.

b, ITC_{dm} activation. Freezing on retrieval: Cre+: 45.7±7.6%; Cre−: 28.5±3.3%; **P*=0.0044

c, Schematic showing the dual-cluster chemogenetic manipulation experiment. An AAV encoding Cre-dependent KORD was targeted to both ITC_{vm} and ITC_{dm} neurons in FoxP2-Cre mice.

d, Freezing behaviour of experimental (Cre+) and control (Cre−) mice; controls were injected with the AAV and administered with the ligand. Arrows and colour-shadings indicate the timing of SalB administration prior to extinction retrieval. Freezing levels on extinction retrieval (Day3): Cre+: 46.4 ± 4.3%; Cre−: 27.3 ± 2.7%; * $P < 0.0001$, repeated measures ANOVA followed by Sidak post-hoc test; N.S.: not significant differences on Day1 or Day2 freezing. Error bars: mean ± SEM

e, Examples of histological validation of KORD-mCitrine expression in ITC_{vm} and ITC_{dm} neurons across multiple anterior-to-posterior coronal sections. Following behavioural experiments, mice were sacrificed and slices (50 μm) cut and stained with an anti-FoxP2 antibody. Scale bar: 200 μm.

f, Heatmaps illustrating virus expression aggregated across Cre+ mice. Scale bar indicates the fraction of animals exhibiting expression at each locus (0: no mice expressed; 1: all mice expressed).

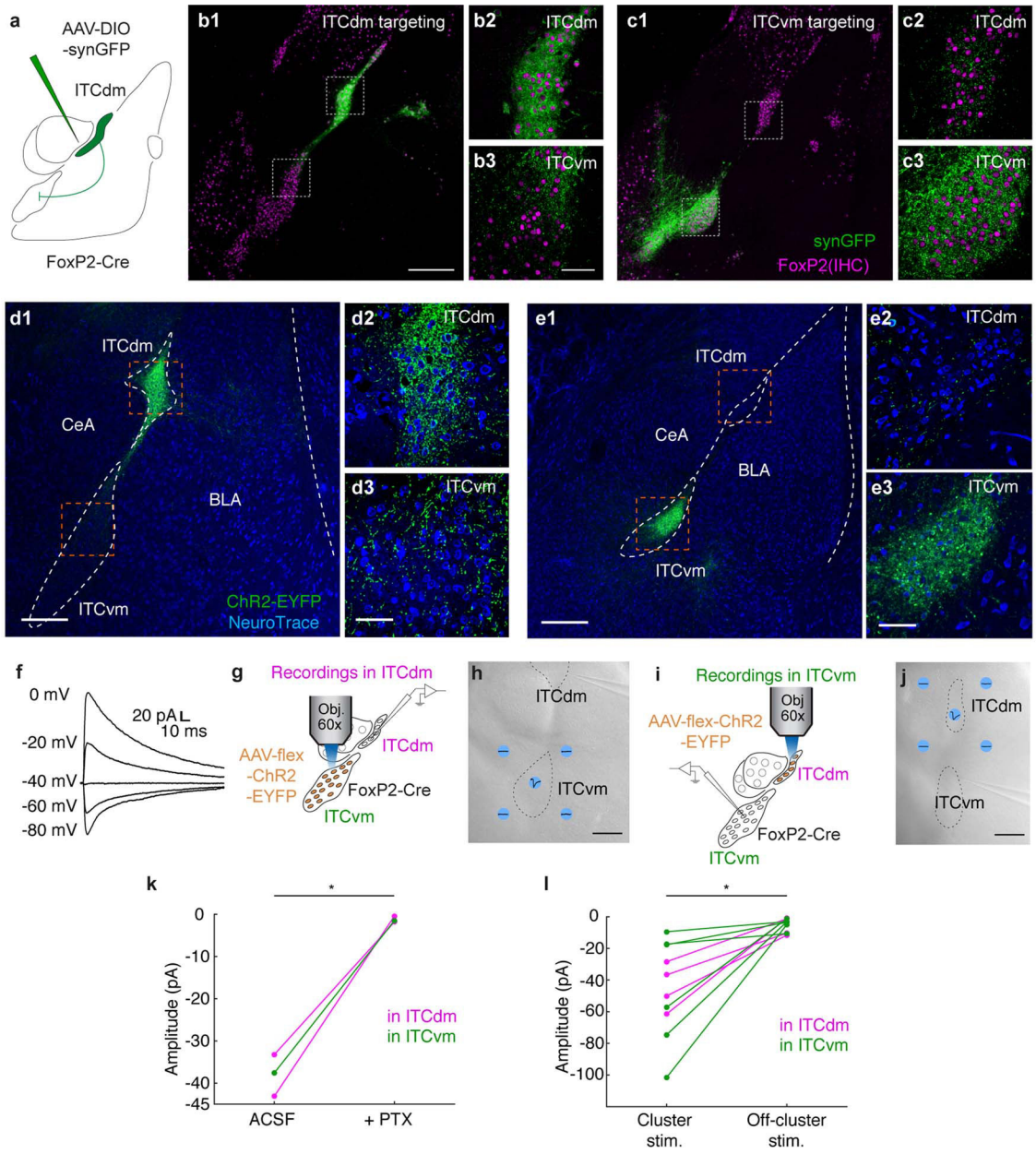

Extended Data Fig. 10 |. Reciprocal inhibitory connections between ITC clusters.

a, Inter-cluster virus-based tracing (ITC_{dm}-targeted example shown, same strategy for ITC_{vm}-targeting). AAV encoding Cre-dependent synaptophysin-GFP targeted to ITC_{dm} or ITC_{vm} neurons in FoxP2-Cre mice.

b,c, Confocal images from ITC_{dm} (**b**) or ITC_{vm} (**c**) injections. FoxP2 expression visualized via immunohistochemistry (IHC). Injections repeated in 5 (ITC_{dm}), and 4 (ITC_{vm}) mice. Scale bars: 500 μm (**b1**, **c1**); 200 μm (**b2–3**, **c2–3**).

d,e, Histological validation of selective ChR2 expression in ITC_{dm} (**d1–3**) and ITC_{vm} (**e1–3**). Scale bars: 500 μm (**d1,e1**); 50 μm (**d3,e3**). Repeated for all the mice shown in Fig. 4.

f, Representative example of IPSCs recorded at different holding potentials from an ITC_{dm} neuron.

g,i, Schematic illustrating *ex vivo* slice electrophysiological experiments with direct cluster stimulation. The ITC_{vm} (**g**) or ITC_{dm} (**i**) cluster was targeted with an AAV encoding Cre-dependent ChR2. Recordings were performed in the other cluster while selectively photostimulating the ChR2-positive cluster or the surrounding area with aperture-restricted stimulation (see Methods).

h,j, Images taken from the recording setup illustrating positions of on- and off-cluster stimulation for ITC_{vm} while recording in ITC_{dm} and vice versa.

k, Summary of PTX application experiments (n = 3 from 3 mice). Magenta lines represent $ITC_{vm} \rightarrow ITC_{dm}$ connections and green lines represent $ITC_{dm} \rightarrow ITC_{vm}$ connections. * $P = 0.005$, paired t-test.

l, Summary of experiments shown in (**g**)-(**j**). On-cluster photostimulation evoked significantly larger IPSCs than off-cluster stimulation. Note, the highest value out of the 4 off-cluster stimulation sites were used. * $P = 0.0016$, paired t-test.

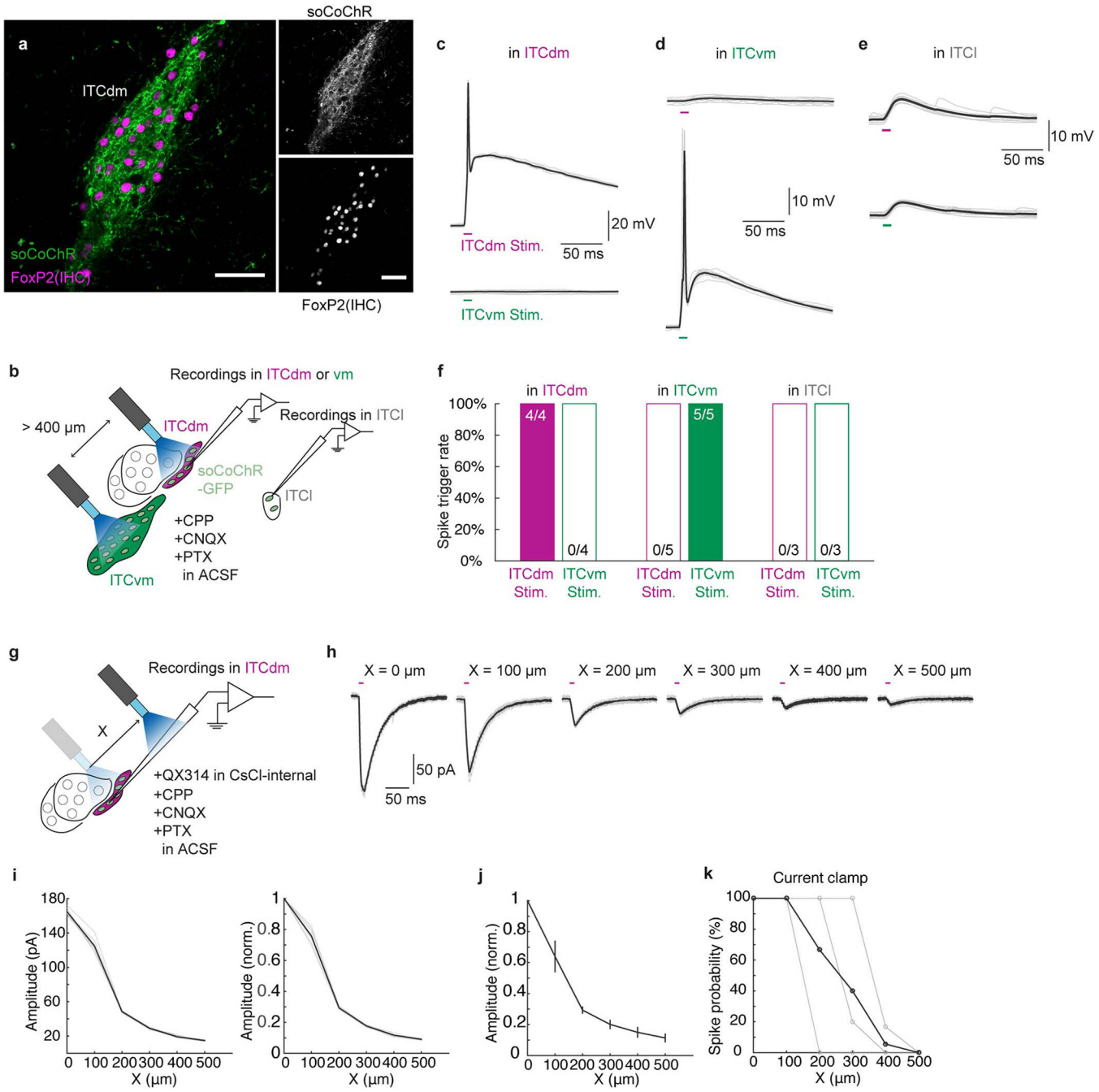

Extended Data Fig. 11 |. Selective *ex vivo* ITC cluster stimulation.

a, Histological validation of selective soCoChR expression. Scale bars: 50 µm. Repeated for N = 3 mice.

b, Schematic illustrating *ex vivo* slice electrophysiological experiments. ITC_{dm} and ITC_{vm} neurons were targeted with an AAV encoding Cre-dependent soCoChR. Two optical fibres for photostimulation were placed above the ITC clusters. Whole-cell recordings were performed from neurons in the ITC_{dm}, ITC_{vm}, and lateral ITC (ITC_l) clusters. To block synaptic currents, CPP (10 µM), CNQX (10 µM), and PTX (100 µM) were applied.

c-e, Example responses to photostimulation of ITC_{dm} or ITC_{vm} clusters recorded under current-clamp configuration from ITC_{dm} (**c**), ITC_{vm} (**d**), and ITC_{l} (**e**) neurons.
f, Summary of experiments shown in **b-e**. All recorded ITC_{dm} and ITC_{vm} neurons fired action potentials selectively in response to photostimulation with the corresponding fibre. ITC_{l} neurons did not fire action potentials upon photostimulation of ITC_{dm} or ITC_{vm} clusters.
g, Schematic illustrating experiments wherein the position of the optical fibre was systematically moved away from the optimal location (X = 0 μm). To block synaptic currents, CPP (10 μM), CNQX (10 μM), and PTX (100 μM) were applied. These experiments further confirm spatial resolution of the photostimulation configuration.
h, Example voltage-clamp recordings from an ITC neuron showing IPSCs evoked at different positions of the optical fibre.
i,*Left*: Quantification of peak IPSC amplitudes of the neuron shown in (**h**). *Right*: Normalized by the value at X = 0 μm.
j, Summary of all recorded neurons (n = 3 from 3 mice).
k, Summary of additionally performed current-clamp recordings (n = 3 from 3 mice).

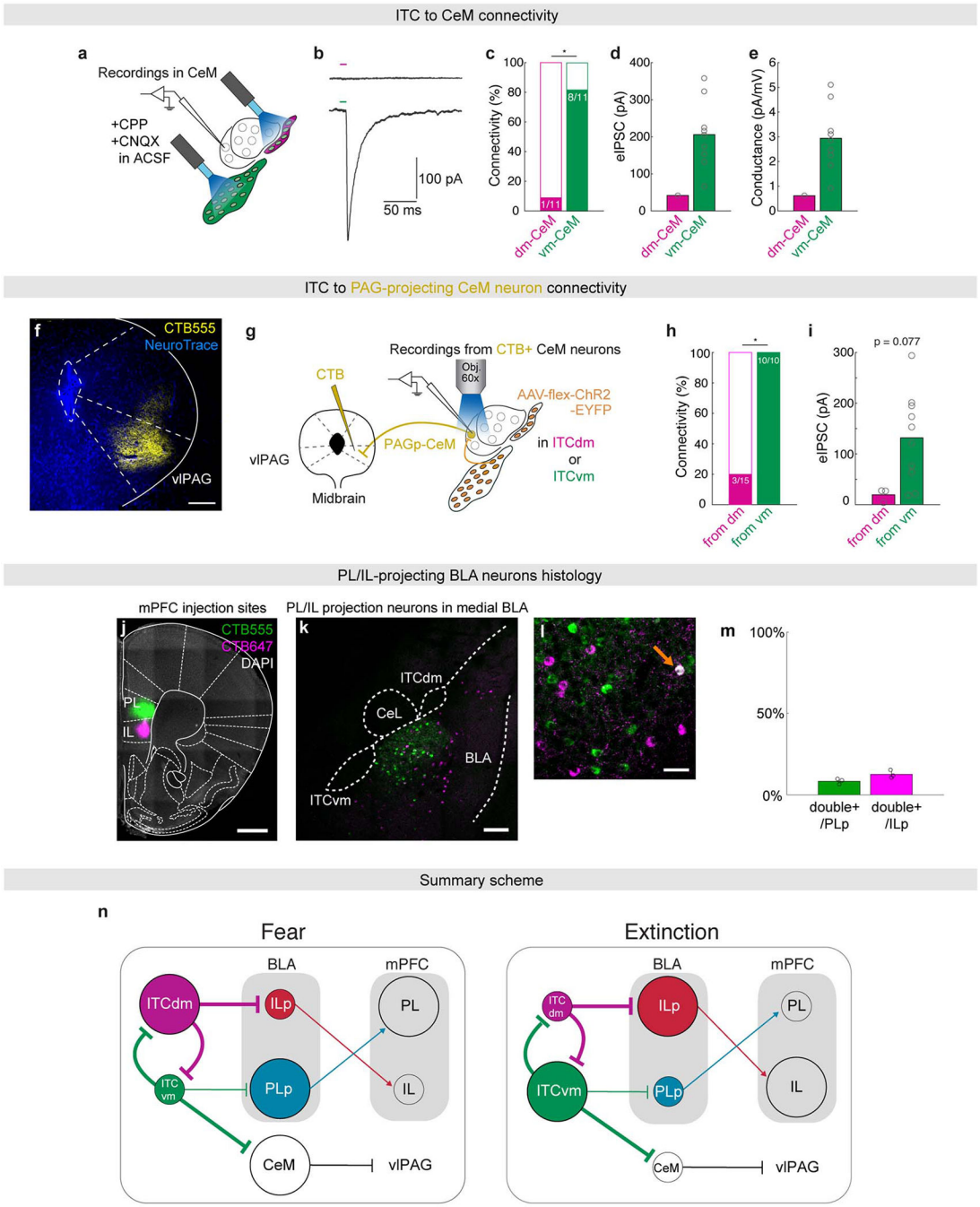

Extended Data Fig. 12 |. ITC to CeM connectivity.

a, Schematic illustrating the experimental design used to assess connectivity between ITC_{dm} or ITC_{vm} neurons and CeM neurons. To isolate IPSCs, CPP (10 μM) and CNQX (10 μM) were applied.

b, Example voltage-clamp recording from a CeM neuron showing selective IPSC elicited by stimulation of the ITC_{vm} but not ITC_{dm}.

c, Summary of connectivity from ITC_{dm} and ITC_{vm} to CeM (n = 11 neurons from 4 mice). * $P = 7.5 \times 10^{-3}$, Fisher's exact test.

d, Evoked IPSC amplitudes recorded from CeM neurons (at −70mV holding potential) in response to stimulation of ITC_{dm} or ITC_{vm} clusters.
e, Synaptic conductance calculated based on IPSC amplitudes recorded at three different holding potentials (−60, −70, and −80 mV).
f, Example injections of CTB555 targeted to the ventrolateral periaqueductal gray (vlPAG). Scale bar: 200 μm.
g, Schematic illustrating the experimental design used to assess connectivity between ITC_{dm} or ITC_{vm} neurons and CeM neurons projecting to the vlPAG. vlPAG-projecting CeM neurons were retrogradely labelled with CTB injections into the vlPAG. Whole-cell recordings were performed in CTB+ CeM neurons while photostimulating incoming axons expressing ChR2-EYFP from either the ITC_{dm} or ITC_{vm}.
h, Summary of connectivity from ITC_{dm} and ITC_{vm} to vlPAG-projecting CeM neurons (n = 15 neurons from 4 mice and n = 10 neurons from 4 mice). * $P = 0.0001$, Fisher's exact test.
i, Evoked IPSC amplitudes recorded from CTB+ CeM neurons (at 0 mV holding potential) in response to stimulation of axons from ITC_{dm} or ITC_{vm}.
j, Example injections of CTB555 and CTB647 targeted to the PL or IL, respectively. Scale bar: 500 μm.
k, Example BLA histology showing PL- (PLp) and IL-projecting (ILp) BLA neurons. Both subpopulations are located in the medial part of the BLA. Scale bar: 200 μm.
l, Mostly non-overlapping PLp and ILp subpopulations; orange arrow indicates an example of a double-labelled neuron. Scale bar: 50 μm.
m, Quantification of double-labelled neurons (N = 3 mice). Error bars: mean ± SEM
n, State-dependent functional changes in amygdala circuitry regulated by ITC clusters. Node size indicates activity levels, connection width represents putative functional connection strength.

Supplementary Material

Refer to Web version on PubMed Central for supplementary material.

Acknowledgements

We thank F. Ferraguti (Univ. Innsbruck) for valuable discussions on ITC cluster nomenclature; J. Felsenberg (FMI), P. Tovote (Univ. Würzburg), and A. Uematsu (RikenCBS / Univ. Tokyo) for reading and commenting on earlier versions of the manuscript; T. Mrsic-Flogel (UCL), M. Häusser (UCL) and B. Roska (FMI, IOB) for discussion and serving as thesis committee members for K.M.H.; E. Susaki (Univ. Tokyo) for sharing the CUBIC protocol; Y. Tanaka (Univ. Tokyo / Harvard) for sharing the NMDG-based slice preparation protocol; L. Choo (Univ. Basel) for slice physiology demonstration; the GENIE Project (HHMI Janelia) for making GCaMP6f, jGCaMP7f, jRGECO1a materials available; Bryan Roth (UNC) for making KORD, DREADD materials available; Karl Deisseroth (Stanford) for making the ChR2 material available; Edward Boyden (MIT) for making the soCoChR material available; All the Lüthi, Holmes, and Ehrlich lab members for discussion and support, especially T. Eichlisberger for excellent animal care; FMI animal facility, microscopy core facility (FAIM), especially L. Gelman and J. Eglinger, and IT department for constant support. This work was supported by the European Research Council (ERC) under the European Union's Horizon 2020 research and innovation program (grant agreement no. 669582), and a Swiss National Science Foundation core grant (310030B_170268) (all to A.Lüthi); by the NIAAA Intramural Research Program (to A.H.); by the German Research Foundation DFG EH 197/3-1 (to I.E.); and by the Novartis Research Foundation.

References

1. Craske MGet al.Anxiety disorders. Nat Rev Dis Primers3, 17024, doi:10.1038/nrdp.2017.24 (2017). [PubMed: 28470168]
2. Duvarci S & Pare D Amygdala microcircuits controlling learned fear. Neuron 82, 966–980, doi:10.1016/j.neuron.2014.04.042 (2014). [PubMed: 24908482]
3. Milad MR & Quirk GJ Fear extinction as a model for translational neuroscience: ten years of progress. Annual review of psychology 63, 129–151, doi:10.1146/annurev.psych.121208.131631 (2012).
4. Orsini CA & Maren S Neural and cellular mechanisms of fear and extinction memory formation. Neurosci Biobehav Rev 36, 1773–1802, doi:10.1016/j.neubiorev.2011.12.014 (2012). [PubMed: 22230704]
5. Tovote P, Fadok JP & Luthi A Neuronal circuits for fear and anxiety. Nature reviews. Neuroscience 16, 317–331, doi:10.1038/nrn3945 (2015). [PubMed: 25991441]
6. Li BCentral amygdala cells for learning and expressing aversive emotional memories. Curr Opin Behav Sci26, 40–45, doi:10.1016/j.cobeha.2018.09.012 (2019). [PubMed: 31011591]
7. LeDoux JEEmotion circuits in the brain. Annual review of neuroscience23, 155–184, doi:DOI 10.1146/annurev.neuro.23.1.155 (2000).
8. Bouton MEContext, ambiguity, and unlearning: sources of relapse after behavioral extinction. Biol Psychiatry52, 976–986, doi:10.1016/s0006-3223(02)01546-9 (2002). [PubMed: 12437938]
9. Herry Cet al.Neuronal circuits of fear extinction. Eur J Neurosci31, 599–612, doi:10.1111/j.1460-9568.2010.07101.x (2010). [PubMed: 20384807]
10. Busti Det al.Different fear states engage distinct networks within the intercalated cell clusters of the amygdala. The Journal of neuroscience : the official journal of the Society for Neuroscience31, 5131–5144, doi:10.1523/JNEUROSCI.6100-10.2011 (2011). [PubMed: 21451049]
11. Collins DR & Pare D Spontaneous and evoked activity of intercalated amygdala neurons. Eur J Neurosci 11, 3441–3448, doi:10.1046/j.1460-9568.1999.00763.x (1999). [PubMed: 10564352]
12. Millhouse OEThe intercalated cells of the amygdala. J Comp Neurol247, 246–271, doi:10.1002/cne.902470209 (1986). [PubMed: 2424941]
13. Waclaw RR, Ehrman LA, Pierani A & Campbell K Developmental origin of the neuronal subtypes that comprise the amygdalar fear circuit in the mouse. The Journal of neuroscience : the official journal of the Society for Neuroscience 30, 6944–6953, doi:10.1523/JNEUROSCI.5772-09.2010 (2010). [PubMed: 20484636]
14. Royer S, Martina M & Pare D An inhibitory interface gates impulse traffic between the input and output stations of the amygdala. The Journal of neuroscience : the official journal of the Society for Neuroscience 19, 10575–10583 (1999). [PubMed: 10575053]
15. Amano T, Unal CT & Pare D Synaptic correlates of fear extinction in the amygdala. Nature neuroscience 13, 489–494, doi:10.1038/nn.2499 (2010). [PubMed: 20208529]
16. Likhtik E, Popa D, Apergis-Schoute J, Fidacaro GA & Pare D Amygdala intercalated neurons are required for expression of fear extinction. Nature 454, 642–645, doi:10.1038/nature07167 (2008). [PubMed: 18615014]
17. Asede D, Bosch D, Luthi A, Ferraguti F & Ehrlich I Sensory inputs to intercalated cells provide fear-learning modulated inhibition to the basolateral amygdala. Neuron 86, 541–554, doi:10.1016/j.neuron.2015.03.008 (2015). [PubMed: 25843406]
18. Manko M, Geracitano R & Capogna M Functional connectivity of the main intercalated nucleus of the mouse amygdala. J Physiol 589, 1911–1925, doi:10.1113/jphysiol.2010.201475 (2011). [PubMed: 21224220]
19. Grewe BFet al.Neural ensemble dynamics underlying a long-term associative memory. Nature543, 670–675, doi:10.1038/nature21682 (2017). [PubMed: 28329757]
20. Luo Ret al.A dopaminergic switch for fear to safety transitions. Nat Commun9, 2483, doi:10.1038/s41467-018-04784-7 (2018). [PubMed: 29950562]
21. Salinas-Hernandez XIet al.Dopamine neurons drive fear extinction learning by signaling the omission of expected aversive outcomes. Elife7, doi:10.7554/eLife.38818 (2018).

22. Strobel C, Marek R, Gooch HM, Sullivan RKP & Sah P Prefrontal and Auditory Input to Intercalated Neurons of the Amygdala. Cell Rep 10, 1435–1442, doi:10.1016/j.celrep.2015.02.008 (2015). [PubMed: 25753409]
23. Herry Cet al.Switching on and off fear by distinct neuronal circuits. Nature454, 600–606, doi:10.1038/nature07166 (2008). [PubMed: 18615015]
24. Pare D & Smith Y GABAergic projection from the intercalated cell masses of the amygdala to the basal forebrain in cats. J Comp Neurol 344, 33–49, doi:10.1002/cne.903440104 (1994). [PubMed: 7520456]
25. Tovote Pet al.Midbrain circuits for defensive behaviour. Nature534, 206–212, doi:10.1038/nature17996 (2016). [PubMed: 27279213]
26. Senn Vet al.Long-range connectivity defines behavioral specificity of amygdala neurons. Neuron81, 428–437, doi:10.1016/j.neuron.2013.11.006 (2014). [PubMed: 24462103]
27. McGarry LM & Carter AG Inhibitory Gating of Basolateral Amygdala Inputs to the Prefrontal Cortex. J Neurosci 36, 9391–9406, doi:10.1523/JNEUROSCI.0874-16.2016 (2016). [PubMed: 27605614]
28. Arruda-Carvalho M & Clem RL Prefrontal-amygdala fear networks come into focus. Front Syst Neurosci 9, 145, doi:10.3389/fnsys.2015.00145 (2015). [PubMed: 26578902]
29. Koyama M & Pujala A Mutual inhibition of lateral inhibition: a network motif for an elementary computation in the brain. Curr Opin Neurobiol 49, 69–74, doi:10.1016/j.conb.2017.12.019 (2018). [PubMed: 29353136]
30. Machens CK, Romo R & Brody CD Flexible control of mutual inhibition: a neural model of two-interval discrimination. Science 307, 1121–1124, doi:10.1126/science.1104171 (2005). [PubMed: 15718474]
31. Felsenberg Jet al.Integration of Parallel Opposing Memories Underlies Memory Extinction. Cell175, 709–722 e715, doi:10.1016/j.cell.2018.08.021 (2018). [PubMed: 30245010]
32. Solomon RL & Corbit JD Opponent-Process Theory of Motivation.1. Temporal Dynamics of Affect. Psychological Review 81, 119–145, doi:DOI 10.1037/h0036128 (1974). [PubMed: 4817611]
33. Zhang X, Kim J & Tonegawa S Amygdala Reward Neurons Form and Store Fear Extinction Memory. Neuron 105, 1077–1093 e1077, doi:10.1016/j.neuron.2019.12.025 (2020). [PubMed: 31952856]
34. Braak H & Braak E Neuronal types in the basolateral amygdaloid nuclei of man. Brain Res Bull 11, 349–365, doi:10.1016/0361-9230(83)90171-5 (1983). [PubMed: 6640364]

Methods References

35. Rousso DLet al.Two Pairs of ON and OFF Retinal Ganglion Cells Are Defined by Intersectional Patterns of Transcription Factor Expression. Cell Rep15, 1930–1944, doi:10.1016/j.celrep.2016.04.069 (2016). [PubMed: 27210758]
36. Guenthner CJ, Miyamichi K, Yang HH, Heller HC & Luo L Permanent genetic access to transiently active neurons via TRAP: targeted recombination in active populations. Neuron 78, 773–784, doi:10.1016/j.neuron.2013.03.025 (2013). [PubMed: 23764283]
37. Chen TWet al.Ultrasensitive fluorescent proteins for imaging neuronal activity. Nature499, 295–300, doi:10.1038/nature12354 (2013). [PubMed: 23868258]
38. Vardy Eet al.A New DREADD Facilitates the Multiplexed Chemogenetic Interrogation of Behavior. Neuron86, 936–946, doi:10.1016/j.neuron.2015.03.065 (2015). [PubMed: 25937170]
39. Armbruster BN, Li X, Pausch MH, Herlitze S & Roth BL Evolving the lock to fit the key to create a family of G protein-coupled receptors potently activated by an inert ligand. Proceedings of the National Academy of Sciences of the United States of America 104, 5163–5168, doi:10.1073/pnas.0700293104 (2007). [PubMed: 17360345]
40. Shemesh OAet al.Temporally precise single-cell-resolution optogenetics. Nature neuroscience20, 1796–1806, doi:10.1038/s41593-017-0018-8 (2017). [PubMed: 29184208]
41. Dana Het al.Sensitive red protein calcium indicators for imaging neural activity. Elife5, doi:10.7554/eLife.12727 (2016).

42. Dana Het al.High-performance calcium sensors for imaging activity in neuronal populations and microcompartments. Nature methods16, 649–657, doi:10.1038/s41592-019-0435-6 (2019). [PubMed: 31209382]
43. Renier Net al.iDISCO: a simple, rapid method to immunolabel large tissue samples for volume imaging. Cell159, 896–910, doi:10.1016/j.cell.2014.10.010 (2014). [PubMed: 25417164]
44. Susaki EAet al.Whole-brain imaging with single-cell resolution using chemical cocktails and computational analysis. Cell157, 726–739, doi:10.1016/j.cell.2014.03.042 (2014). [PubMed: 24746791]
45. Federico Claudi ALT, Tiago Branco. Brainrender. A python based software for visualisation of neuroanatomical and morphological data. bioRxiv, doi:doi:10.1101/2020.02.23.961748 (2020).
46. Ghosh KKet al.Miniaturized integration of a fluorescence microscope. Nature methods8, 871–878, doi:10.1038/nmeth.1694 (2011). [PubMed: 21909102]
47. Franklin KBJ & Paxinos G The mouse brain in stereotaxic coordinates. (Academic Press, 1997).
48. Bukalo Oet al.Prefrontal inputs to the amygdala instruct fear extinction memory formation. Sci Adv1, doi:10.1126/sciadv.1500251 (2015).
49. Petreanu L, Huber D, Sobczyk A & Svoboda K Channelrhodopsin-2-assisted circuit mapping of long-range callosal projections. Nature neuroscience 10, 663–668, doi:10.1038/nn1891 (2007). [PubMed: 17435752]
50. Tanaka Y, Tanaka Y, Furuta T, Yanagawa Y & Kaneko T The effects of cutting solutions on the viability of GABAergic interneurons in cerebral cortical slices of adult mice. J Neurosci Methods 171, 118–125, doi:10.1016/j.jneumeth.2008.02.021 (2008). [PubMed: 18430473]
51. Ting JT, Daigle TL, Chen Q & Feng G Acute brain slice methods for adult and aging animals: application of targeted patch clamp analysis and optogenetics. Methods Mol Biol 1183, 221–242, doi:10.1007/978-1-4939-1096-0_14 (2014). [PubMed: 25023312]
52. Lerner TNet al.Intact-Brain Analyses Reveal Distinct Information Carried by SNc Dopamine Subcircuits. Cell162, 635–647, doi:10.1016/j.cell.2015.07.014 (2015). [PubMed: 26232229]
53. Gunaydin LAet al.Natural neural projection dynamics underlying social behavior. Cell157, 1535–1551, doi:10.1016/j.cell.2014.05.017 (2014). [PubMed: 24949967]
54. Lopes Get al.Bonsai: an event-based framework for processing and controlling data streams. Front Neuroinform9, 7, doi:10.3389/fninf.2015.00007 (2015). [PubMed: 25904861]
55. An Bet al.Amount of fear extinction changes its underlying mechanisms. Elife6, doi:10.7554/eLife.25224 (2017).
56. Baek Jet al.Neural circuits underlying a psychotherapeutic regimen for fear disorders. Nature566, 339–343, doi:10.1038/s41586-019-0931-y (2019). [PubMed: 30760920]
57. Pnevmatikakis EA & Giovannucci A NoRMCorre: An online algorithm for piecewise rigid motion correction of calcium imaging data. J Neurosci Methods 291, 83–94, doi:10.1016/j.jneumeth.2017.07.031 (2017). [PubMed: 28782629]
58. Hagihara KM, Murakami T, Yoshida T, Tagawa Y & Ohki K Neuronal activity is not required for the initial formation and maturation of visual selectivity. Nature neuroscience 18, 1780–1788, doi:10.1038/nn.4155 (2015). [PubMed: 26523644]
59. Kerlin AM, Andermann ML, Berezovskii VK & Reid RC Broadly tuned response properties of diverse inhibitory neuron subtypes in mouse visual cortex. Neuron 67, 858–871, doi:10.1016/j.neuron.2010.08.002 (2010). [PubMed: 20826316]
60. Grundemann Jet al.Amygdala ensembles encode behavioral states. Science364, doi:10.1126/science.aav8736 (2019).

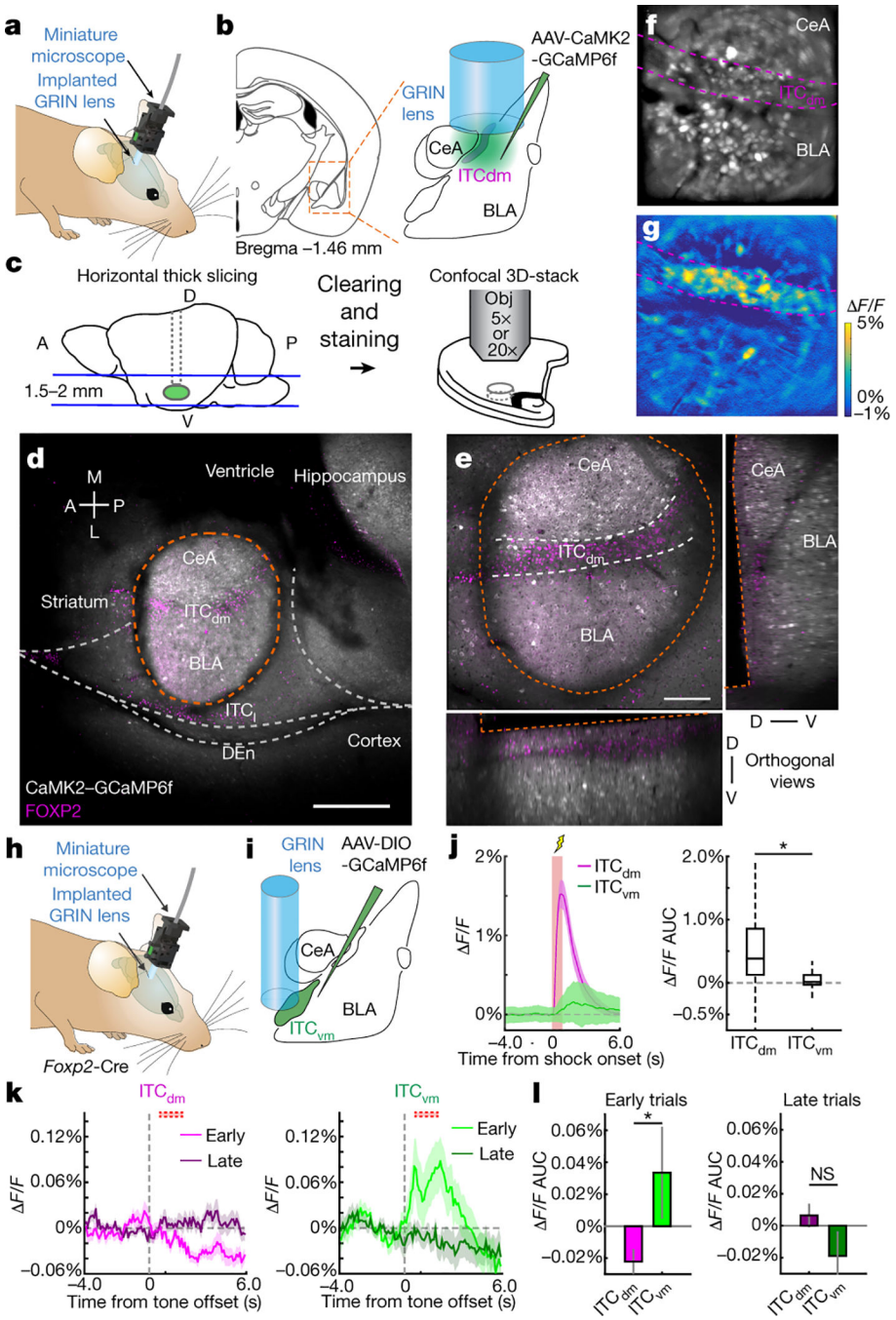

Fig. 1 |. ITC clusters differentially signal the presence and absence of an aversive stimulus.

a, Endoscopic imaging with a miniaturized microscope in a freely-moving mouse.

b, AAV encoding CaMK2-GCaMP6f targeted to CeA, BLA and ITC_{dm}. GRIN lens implanted above injection site.

c, Post-hoc identification of ITC_{dm} neurons. *Left:* FOV-containing horizontal sections cleared (CUBIC protocol) and immunostained with anti-FoxP2 antibody. *Right:* Confocal images of sections. Gray lines: GRIN lens position.

d, Confocal image of tissue acquired with 5x objective (from mouse in **f,g**). Orange dotted line indicates outline of GRIN lens implanted area. Scale bar: 500 μm. Str.: Striatum; Vent.: Ventricle; DEn: Dorsal endopiriform nucleus; Hip.: Hippocampus; Sub.: Subiculum

e, Sample shown in **d**, acquired with 20x objective. XZ and YZ orthogonal views visualized in an isotropic manner. Scale bar: 250 μm. See also Supplementary Movie 2. Repeated for N=9 mice.

f, Maximum-intensity projection image of BLA, CeA, and ITC_{dm} neurons acquired with a miniature microscope. Dashed magenta lines indicate FoxP2-positive area in **f** with dashed white lines (identified as ITC_{dm}). Image approximates to 600 × 600 μm.

g, A ΔF/F map showing clustered ITC_{dm} activation. See also Supplementary Movie 3.

h, Miniature microscope imaging in a freely-moving mouse.

i, AAV encoding CAG-DIO-GCaMP6f was targeted to ITC_{vm}. GRIN lens implanted above injection site.

j,*Left:* Averaged Ca^{2+} footshock US responses (red shading) in all recorded ITC_{dm} (magenta, n=271 neurons, 9 mice) and ITC_{vm} neurons (green, n=372 neurons, 6 mice). *Right:* Averaged ΔF/F values. $*P=2.1 \times 10^{-32}$, Wilcoxon rank-sum test. Box plot represents median, 25th and 75th percentiles, whiskers represent data-range.

k, Trial-averaged ΔF/F Ca^{2+} timecourse of all recorded ITC_{dm} (left) or ITC_{vm} (right) neurons during US omission on first and last 5 trials. Dotted red boxes indicate expected US delivery.

l, Averaged ΔF/F responses to US omission on first (left) and last 5 trials. Error bars: mean±SEM.

$*P=0.0039$, N.S.: $P=0.98$, Two-sided Wilcoxon rank-sum test.

Data in **j-l** obtained from same animals in Fig. 2.

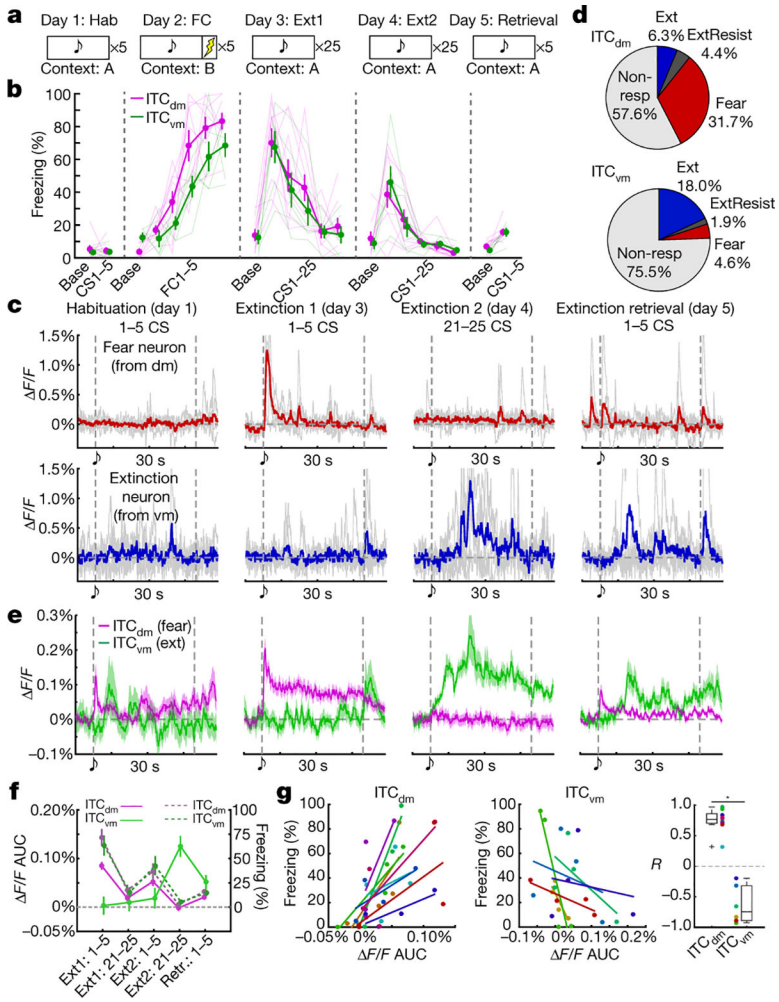

Fig. 2 |. CS responses of ITC clusters parallel the switch from high to low fear state.

a, 5-day fear conditioning and extinction paradigm.

b, Freezing in ITC_{dm} (magenta, N=9) and ITC_{vm} targeted (green, N=6) mice. ITCdm: FC1–5: P=4.7*10^{-9} (ascend); Ext1 CS1–25: P=4.2*10^{-7} (descend); Ext2 CS1–25: P=1.9*10^{-9} (descend); ITCvm: FC1–5: P=1.8*10^{-7} (ascend); Ext1 CS1–25: P=3.9*10^{-5} (descend); Ext2 CS1–25: P=7.5*10^{-6} (descend); Jonckheere-Terpstra test for trend. Error bars: mean±SEM

c, Ca^{2+} traces of Fear and Extinction neurons from ITC_{dm} and ITC_{vm}, respectively. 5-trial averaged traces in colour and traces from individual trials in gray.

d, Fractions of Fear, Extinction, and Extinction Resistant neurons in ITC_{dm} (n=271 neurons, 9 mice) and ITC_{vm} (n=372 neurons, 6 mice). P=6.3 × 10^{-20}, Chi-squared test. Fear neurons: P<0.01; Extinction neurons: P<0.01; Extinction Resistant neurons: P>0.10.

e, Averaged Ca^{2+} responses to CSs in ITC_{dm} fear (magenta, n=86) and ITC_{vm} extinction (green, n=67) neurons. Vertical dotted lines indicate CS onset and offset. For responses in entire recorded population, including task phase-classified neurons shown here, aligned and baseline-normalized to CS-offset, see Fig. 1k.

f, Averaged ΔF/F values (solid lines) and freezing (dotted lines) from ITC_{dm} and ITC_{vm} targeted mice during each test stage. Error bars: mean±SEM

g, Relationships between 5-trial averaged ΔF/F values (as in panel **f**) and freezing during each test stage, for ITC_{dm} Fear (*Left*) and ITC_{vm} Extinction (*Center*) neurons. Data points (5 per mouse, 1 per stage) and lines (linear regression fitted) colour-coded by individual mouse (ITC_{dm}: N=9; ITC_{vm}: N=6). R (correlation coefficient) fitted lines (*Right*); dots coloured as in left panels. **P*=4.0 × 10−4, Wilcoxon rank-sum test. Box plot represents median, 25th and 75th percentiles, whiskers represent data-range.

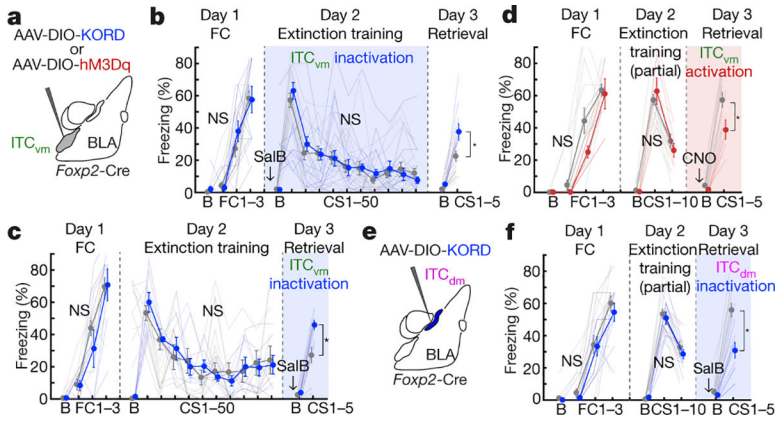

Fig. 3 |. ITC clusters differentially and bidirectionally regulate fear extinction.

a,e, Chemogenetic manipulations of individual ITCs.

b,c, ITC_{vm} inactivation. Freezing in Cre+ and Cre− controls (injected with same AAV and ligand). Arrows and colour-shadings indicate timing of SalB administration relative to full (50-trial) extinction training (**b**) or retrieval (**c**). Freezing on retrieval in **b**: Cre+: 37.6±5.2%; Cre−: 22.5±3.1%; **P*=0.0013; in **c**: Cre+: 45.8±2.7%; Cre−: 27.3±4.9%; **P*=0.0005

d, ITC_{vm} activation. Freezing in Cre+ and Cre− mice. Freezing on retrieval: Cre+: 38.9±6.1%; Cre−: 57.3±4.6%; **P*=0.0079

f, ITC_{dm} inactivation. Freezing on retrieval: Cre+: 30.9±4.8%; Cre−: 55.8±4.2%; **P*<0.0001 Repeated measures ANOVA, Sidak post-hoc test. Error bars: mean±SEM. N.S.: not significant differences on Day1 or Day2 freezing.

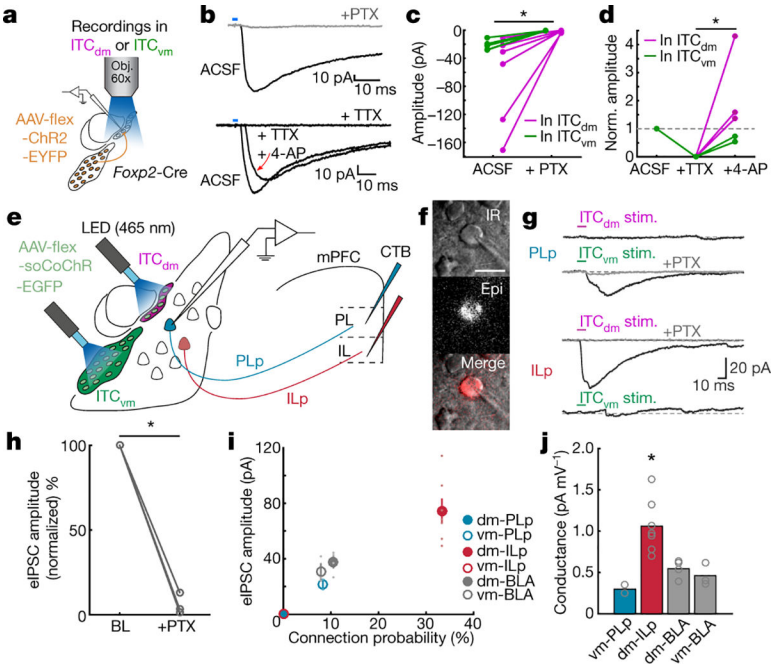

Fig. 4 |. ITC clusters exert reciprocal inhibition and selective control over extinction-regulating amygdala outputs.

a, Inter-cluster *ex vivo* electrophysiology. AAV encoding Cre-dependent ChR2-EYFP targeted to ITC_{vm} or ITC_{dm} neurons in FoxP2-Cre mice. Recordings in one ITC cluster while photostimulating ChR2-EYFP-expressing axons from the other cluster.

b, (Top): Example IPSC (−70mV holding potential) evoked by photostimulating ChR2-EYFP-expressing axons. Picrotoxin (PTX) abolished IPSCs. (Bottom): IPSC (−70mV holding potential) evoked by photostimulating ChR2-expressing axons. Mono-synaptic IPSCs were isolated by subsequent application of Tetrodotoxin (TTX)/TTX + 4-Aminopyridine (4-AP).

c, PTX experiments. Magenta lines: ITC_{vm}→ITC_{dm} connections (n=6 neurons, 6 mice); green lines= ITC_{dm}→ITC_{vm} connections (n=5 neurons, 4 mice). **P*=0.011, paired t-test.

d, TTX + 4-AP application (ITC_{vm}→ITC_{dm}: n=3 neurons, 3 mice, ITC_{dm}→ITC_{vm}: n=2 neurons, 2 mice). **P*=0.029, one-way ANOVA and Tukey-Kramer.

e, Long-range circuit *ex vivo* electrophysiology. ITC_{dm} and ITC_{vm} neurons targeted with AAV encoding Cre-dependent soCoChR in FoxP2-Cre mice. Two optical fibres placed above ITC clusters. PL- and IL-projecting BLA neurons retrogradely labelled with CTB.

f, CTB-positive BLA neuron under the microscope for slice recordings. Scale bar: 20 μm.

g, IPSCs recorded from PL- (PLp) and IL-projecting (ILp) BLA neurons (−70mV holding potential) evoked by photostimulating soCoChR-expressing ITC clusters. Picrotoxin (PTX) application blocked IPSCs.

h, Mean normalized evoked IPSC before and after PTX application (ITCdm→ILp, ITCvm→PLp, ITCvm→unidentified, total: n=3 neurons, 3 mice). **P*=0.030, paired t-test. BL: Baseline.

i, Connection probability and mean evoked IPSC amplitudes from ITC clusters to PL- or IL-projecting and unidentified (CTB−) BLA neurons (PLp: PL-projecting, n = 24 neurons; ILp:

IL-projecting, n=21 neurons; unidentified, n=38 neurons). ITCdm→PLp and ITCvm→ILp connections were not observed: datapoints superimposed at **o**.

j, Synaptic conductance of evoked IPSCs from connected neurons. Slopes calculated from IPSC amplitudes acquired at three different holding potentials (−60, −70, −80mV). **P*=0.0028, one-way ANOVA, Tukey-Kramer.